

# Isotopic constraints on heterogeneous sulfate production in Beijing haze

Pengzhen He<sup>1</sup>, Becky Alexander<sup>2</sup>, Lei Geng<sup>1</sup>, Xiyuan Chi<sup>1</sup>, Shidong Fan<sup>1</sup>, Haicong Zhan<sup>1</sup>, Hui Kang<sup>1</sup>, Guangjie Zheng<sup>3†</sup>,  
Yafang Cheng<sup>3,4</sup>, Hang Su<sup>4,3</sup>, Cheng Liu<sup>1,5,6</sup>, Zhouqing Xie<sup>1,5,6\*</sup>

<sup>1</sup>Anhui Province Key Laboratory of Polar Environment and Global Change, School of Earth and Space Sciences, University of Science and Technology of China, Hefei, Anhui 230026, China.

<sup>2</sup>Department of Atmospheric Sciences, University of Washington, Seattle, WA 98195, USA.

<sup>3</sup>Multiphase Chemistry Department, Max Planck Institute for Chemistry, Mainz 55128, Germany.

<sup>4</sup>Jinan University, Institute for Environment and Climate Research, Guangzhou, Guangdong 511443, China.

<sup>5</sup>Key Lab of Environmental Optics and Technology, Anhui Institute of Optics and Fine Mechanics, Chinese Academy of Sciences, Hefei, Anhui 230031, China.

<sup>6</sup>Center for Excellence in Urban Atmospheric Environment, Institute of Urban Environment, Chinese Academy of Sciences, Xiamen, Fujian 361021, China.

\*Corresponding to: Zhouqing Xie ([zqxie@ustc.edu.cn](mailto:zqxie@ustc.edu.cn))

†: Now at: Atmospheric Sciences Division, Brookhaven National Laboratory, Upton, NY 11973, USA.

**Abstract.** Discerning mechanisms of sulfate formation during fine-particle pollution (referred to as haze hereafter) in Beijing is important for understanding the rapid evolution of haze and for developing cost-effective air pollution mitigation strategies. Here we present the first observations of the oxygen-17 excess of PM<sub>2.5</sub> sulfate ( $\Delta^{17}\text{O}(\text{SO}_4^{2-})$ ) collected in Beijing haze from October 2014 to January 2015 to constrain possible sulfate formation pathways. Throughout the sampling campaign, the 12h-averaged PM<sub>2.5</sub> concentrations ranged from 16 to 323  $\mu\text{g m}^{-3}$  with a mean of  $(141 \pm 88 \text{ (1}\sigma)) \mu\text{g m}^{-3}$ , with  $\text{SO}_4^{2-}$  representing 8–25 % of PM<sub>2.5</sub> mass. The observed  $\Delta^{17}\text{O}(\text{SO}_4^{2-})$  varied from 0.1 ‰ to 1.6 ‰ with a mean of  $(0.9 \pm 0.3) \text{ ‰}$ .  $\Delta^{17}\text{O}(\text{SO}_4^{2-})$  increased with PM<sub>2.5</sub> levels in October 2014 while the opposite trend was observed in November 2014 to January 2015. Our estimate suggested that in-cloud reactions dominated sulfate production in polluted days (PD,  $\text{PM}_{2.5} \geq 75 \mu\text{g m}^{-3}$ ) of Case II in October 2014 due to the relatively high cloud liquid water content (LWC), with a fractional contribution up to 68 %. However, heterogeneous sulfate production ( $P_{\text{het}}$ ) on aerosols was estimated to dominate sulfate formation during PD of other cases, with a fractional contribution of  $(48 \pm 5) \text{ ‰}$ . For the specific mechanisms of heterogeneous oxidation of  $\text{SO}_2$ , chemical reaction kinetics calculations suggested S(IV) ( $= \text{SO}_2 \text{ H}_2\text{O} + \text{HSO}_3^- + \text{SO}_3^{2-}$ ) oxidation by  $\text{H}_2\text{O}_2$  in aerosol water accounted for 5–13 % of  $P_{\text{het}}$ . The relative importance of heterogeneous sulfate production by other mechanisms was constrained by our observed  $\Delta^{17}\text{O}(\text{SO}_4^{2-})$ . Heterogeneous sulfate production via S(IV) oxidation by  $\text{O}_3$  was estimated to contribute 21–22 % of  $P_{\text{het}}$  on average. Heterogeneous sulfate production pathways that result in zero- $\Delta^{17}\text{O}(\text{SO}_4^{2-})$ , such as

31 S(IV) oxidation by  $\text{NO}_2$  in aerosol water and/or by  $\text{O}_2$  via a radical chain mechanism, contributed the remaining 66–73 % of  
 32  $P_{\text{het}}$ . The assumption about the thermodynamic state of aerosols (stable or metastable) was found to significantly influence the  
 33 calculated aerosol pH ( $7.6 \pm 0.1$  or  $4.7 \pm 1.1$ , respectively), and thus influence the relative importance of heterogeneous sulfate  
 34 production via S(IV) oxidation by  $\text{NO}_2$  and by  $\text{O}_2$ . Our calculation suggests sulfate formation via  $\text{NO}_2$  oxidation can be the  
 35 dominant pathway in aerosols at high pH-conditions calculated assuming stable state while S(IV) oxidation by  $\text{O}_2$  can be the  
 36 dominant pathway providing that highly acidic aerosols ( $\text{pH} \leq 3$ ) exist. Our results also illustrate the utility of  $\Delta^{17}\text{O}(\text{SO}_4^{2-})$  for  
 37 quantifying sulfate formation pathways and its inclusion in models may improve our understanding of rapid sulfate formation  
 38 during haze events.

## 39 1 Introduction

40 Frequent occurrence of haze events in Beijing and throughout the North China Plain (NCP) during cold seasons is a health  
 41 threat for round 400 million people living there. High concentrations of  $\text{PM}_{2.5}$  (particulate matter with an aerodynamic  
 42 diameter less than  $2.5 \mu\text{m}$ ), of which the daily average can exceed  $300 \mu\text{g m}^{-3}$  during severe haze (He et al., 2014; Jiang et al.,  
 43 2015), contribute to cardiovascular morbidity and mortality (Brook et al., 2010; Cheng et al., 2013). As one of the major  
 44 components of  $\text{PM}_{2.5}$ , sulfate is of particular concern due to its high concentrations in haze days (Zheng et al., 2015b; Zheng et  
 45 al., 2015a) and its key role in the climate system (Seinfeld and Pandis, 2012). Hourly sulfate concentrations can exceed  $100 \mu\text{g}$   
 46  $\text{m}^{-3}$  and account for up to one quarter of  $\text{PM}_{2.5}$  mass during severe haze (Zheng et al., 2015a). However, due to the generally  
 47 low solar radiation and cloud liquid water content (LWC) during haze (Zheng et al., 2015a; Wang et al., 2014), conventional  
 48 sulfate formation via OH oxidation in the gas-phase and from aqueous-phase  $\text{SO}_2$  (referred to as S(IV) =  $\text{SO}_2 \cdot \text{H}_2\text{O} + \text{HSO}_3^- +$   
 49  $\text{SO}_3^{2-}$ ) oxidation by  $\text{H}_2\text{O}_2$  (McArdle and Hoffmann, 1983),  $\text{O}_3$  (Hoffmann and Calvert, 1985), and  $\text{O}_2$  via a radical chain  
 50 mechanism initiated by transition metal ions (TMIs) in clouds (Ibusuki and Takeuchi, 1987; Alexander et al., 2009; Harris et  
 51 al., 2013) cannot explain the observed high sulfate concentrations (Zheng et al., 2015a). To explain the observed high sulfate  
 52 concentrations during haze in Beijing and NCP, recent studies have suggested that heterogeneous reactions on/in  
 53 aerosols/aerosol water are potentially important (He et al., 2014; Hung and Hoffmann, 2015; Cheng et al., 2016; Wang et al.,  
 54 2016; Zheng et al., 2015a; Zheng et al., 2015b; Wang et al., 2014). In particular, Zheng et al. (2015a) largely improved the  
 55 underestimate of modelled sulfate concentrations in 2013 Beijing haze by using a relative humidity (RH)-dependent uptake  
 56 coefficient ( $\gamma$ ) of  $\text{SO}_2$  on aerosols, without knowing the specific mechanisms of heterogeneous oxidation of  $\text{SO}_2$ . Calculations  
 57 by Guo et al. (2017) suggest heterogeneous oxidation of  $\text{SO}_2$  in Beijing maybe dominated by  $\text{O}_2$  via a radical chain mechanism  
 58 initiated by TMIs. Laboratory work has suggested  $\text{SO}_2$  oxidation by  $\text{O}_3$  on mineral dust is a significant pathway for sulfate  
 59 production (Li et al., 2006), but its role in Beijing haze has not been determined. More recently, Hung and Hoffmann (2015)  
 60 proposed that rapid S(IV) oxidation by  $\text{O}_2$  via a radical chain mechanism on acidic microdroplets ( $\text{pH} \leq 3$ ) could be responsible

for heterogeneous sulfate production in Beijing haze, while Cheng et al. (2016) suggested that S(IV) oxidation by NO<sub>2</sub> (Lee and Schwartz, 1982; Clifton et al., 1988) in aerosol water could be important due to the high RH and NO<sub>2</sub> concentrations during severe haze in NCP. Due to the strong pH-dependence of SO<sub>2</sub> oxidation and the large variability of model calculated aerosol pH in Beijing haze (Cheng et al., 2016; Wang et al., 2016; Liu et al., 2017), the relative importance of heterogeneous SO<sub>2</sub> oxidation is difficult to constrain.

The oxygen-17 excess ( $\Delta^{17}\text{O}$ ) of sulfate, defined as  $\Delta^{17}\text{O} = \delta^{17}\text{O} - 0.52 \times \delta^{18}\text{O}$  wherein  $\delta^X\text{O} = ((^X\text{O}/^{16}\text{O})_{\text{sample}}/(^X\text{O}/^{16}\text{O})_{\text{VSMOW}} - 1)$  with X = 17 or 18 and VSMOW referring to Vienna Standard Mean Ocean Water (Matsuhisa et al., 1978), is a useful tool for estimating the relative importance of different sulfate formation pathways because each oxidant transfers its  $\Delta^{17}\text{O}$  signature to the product (Table 1) through SO<sub>2</sub> oxidation (Savarino et al., 2000). SO<sub>2</sub> has  $\Delta^{17}\text{O} = 0$  ‰ due to the rapid isotopic exchange with abundant vapour water whose  $\Delta^{17}\text{O}$  is near 0 ‰ (Holt et al., 1981). S(IV) oxidation by H<sub>2</sub>O<sub>2</sub> and O<sub>3</sub> leads to  $\Delta^{17}\text{O}(\text{SO}_4^{2-}) = 0.7$  ‰ and 6.5 ‰, respectively, on the basis of  $\Delta^{17}\text{O}(\text{H}_2\text{O}_2) = 1.4$  ‰ (Savarino and Thiemens, 1999) and assuming  $\Delta^{17}\text{O}(\text{O}_3) = 26$  ‰ (Vicars and Savarino, 2014; Ishino et al., 2017). Other sources of sulfate exhibit  $\Delta^{17}\text{O}(\text{SO}_4^{2-})$  at or near 0 ‰. Specifically, sulfate directly emitted from natural and anthropogenic sources or formed by OH and O<sub>2</sub> oxidation has  $\Delta^{17}\text{O}(\text{SO}_4^{2-})$  values at or near 0 ‰ (Dubey et al., 1997; Luz and Barkan, 2005; Lee et al., 2002; Bao et al., 2000). Sulfate produced by NO<sub>2</sub> oxidation is suggested to occur either via a radical chain mechanism (Shen and Rochelle, 1998), via oxygen-atom transfer from OH<sup>-</sup> (Clifton et al., 1988), or from O<sub>2</sub> based on experimental results of He et al. (2014), resulting in  $\Delta^{17}\text{O}(\text{SO}_4^{2-}) = 0$  ‰. Once formed, atmospheric sulfate does not undergo further isotopic exchange, and  $\Delta^{17}\text{O}(\text{SO}_4^{2-})$  will not be altered by mass-dependent processes such as deposition.

In this work, first observations of PM<sub>2.5</sub>  $\Delta^{17}\text{O}(\text{SO}_4^{2-})$  during haze events from October 2014 to January 2015 in Beijing are reported, contributions of O<sub>3</sub> and H<sub>2</sub>O<sub>2</sub> oxidation in heterogeneous sulfate formation are quantified, and the roles of NO<sub>2</sub> and O<sub>2</sub> oxidation are explored.

## 2 Materials and Methods

### 2.1 Sampling and atmospheric observations

A high volume air sampler (model TH-1000C II, Tianhong Instruments Co., Ltd, China) with quartz microfiber filter (Whatman Inc., UK, pre-combusted at 450 °C for 4 h) was used to collect PM<sub>2.5</sub> samples at a flow rate of 1.05 m<sup>3</sup> min<sup>-1</sup> from October 2014 to January 2015. The collections lasted for 12 h (08:00–20:00 LT or 20:00–08:00 LT) for each sample. The sample site is located on the rooftop of the First Teaching Building at the campus of University of the Chinese Academy of Sciences (40.41 °N, 116.68 °E, around 20 m from the ground) in Beijing, around 60 km northeast of downtown. Hourly PM<sub>2.5</sub>, SO<sub>2</sub>, NO<sub>2</sub> and O<sub>3</sub> concentrations were observed at Huairou station (40.33 °N, 116.63 °E) by Beijing Municipal Environmental Monitoring Center, which is about 10 km from our aerosol sampling site. The concentration of atmospheric H<sub>2</sub>O<sub>2</sub> was not

observed in our campaign, but long-term observations from March to November in Beijing shows a good correlation between  $\text{H}_2\text{O}_2$  concentrations (ppb) and air temperature ( $T$ , in  $^{\circ}\text{C}$ ) according to  $[\text{H}_2\text{O}_2] = 0.1155 \times e^{(0.0846 \times T)}$  (Fu, 2014). In the present study,  $\text{H}_2\text{O}_2$  concentration was estimated from our measured  $T$  with the above empirical equation. Our calculated  $\text{H}_2\text{O}_2$  concentration based on this formula in October and November 2014 is respectively  $(0.32 \pm 0.08)$  ppb and  $(0.17 \pm 0.04)$  ppb, comparable to the observed values of  $(0.44 \pm 0.18)$  ppb and  $(0.38 \pm 0.11)$  ppb, respectively in October and November 2013 (Fu, 2014). Meteorological data including  $T$  and relative humidity (RH) were recorded by an automatic weather station (model MetPak with integrated wind sonic, Gill Instruments Limited, UK). Time reported in this paper is local time ( $\text{LT} = \text{UTC} + 8$ ).

## 2.2 Measurements of ions and isotope ratios

The measurements of ions were conducted in Anhui Province Key Laboratory of Polar Environment and Global Change in the University of Science and Technology of China. A detailed description of the method for chemical analysis of  $\text{NH}_4^+$ ,  $\text{K}^+$ ,  $\text{Ca}^{2+}$ ,  $\text{Na}^+$ ,  $\text{Mg}^{2+}$ ,  $\text{SO}_4^{2-}$ ,  $\text{NO}_3^-$  and  $\text{Cl}^-$  can be found in the literature (Ye et al., 2015). Briefly, ions were extracted from a part ( $2 \text{ cm} \times 2 \text{ cm}$ ) of each filter with 20 ml of Millipore water ( $\geq 18 \text{ M}\Omega$ ) by sonication for 80 min in an ice water bath. Insoluble substances in the extract were filtered with  $0.45 \mu\text{m}$  filters before analysis. The pH of filtrates was measured by an ion activity meter (model PXS-215, Shanghai INESA Scientific Instrument Co., Ltd., China). And the ion concentrations were analysed using Dionex ICS-2100 ion chromatograph system (Thermo Fisher Scientific Inc., USA). Typical analytical precision by our instrument is better than 10 % RSD (relative standard deviation) for all ions (Chen et al., 2016). The preparation and measurements of  $\Delta^{17}\text{O}(\text{SO}_4^{2-})$  were conducted in Isolab (<https://isolab.ess.washington.edu/isolab/>) at the University of Washington, USA. A detailed description of the method can be found in the literature (Savarino et al., 2001; Geng et al., 2013; Chen et al., 2016; Alexander et al., 2012). Briefly,  $\text{PM}_{2.5}$  sample filters were dissolved in Millipore water ( $\geq 18 \text{ M}\Omega$ ) and the insoluble substances were filtered. Pre-packed ion capture cartridges (Alltech Maxi-Clean IC-RP SPE) were used for the first step of removal of organics. Cations in the samples were replaced with sodium using a cation exchange resin and 30 %  $\text{H}_2\text{O}_2$  solution was added as the second step of removal of organics. Excess  $\text{H}_2\text{O}_2$  was removed via evaporation and  $\text{SO}_4^{2-}$  was separated from other anions (e.g.,  $\text{NO}_3^-$ ) by ion chromatography. After ion separation,  $\text{SO}_4^{2-}$  was converted to  $\text{Ag}_2\text{SO}_4$ , dried, and then pyrolyzed at  $1000^{\circ}\text{C}$  in an elemental analyzer to form  $\text{Ag}(\text{s})$ ,  $\text{SO}_2(\text{g})$ , and  $\text{O}_2(\text{g})$ . The produced gases were carried by He gas to pass through a liquid nitrogen trap to remove  $\text{SO}_2$ , and then a GC to further purify the  $\text{O}_2$  gas which was finally induced to a mass spectrometer (Thermo Scientific MAT 253). Masses of 32, 33 and 34 of  $\text{O}_2$  were measured to determine  $\delta^{17}\text{O}$  and  $\delta^{18}\text{O}$  and then  $\Delta^{17}\text{O}$  was calculated. The precision of  $\Delta^{17}\text{O}$  measurements in our method is  $\pm 0.3 \text{ ‰}$  based on replicate analysis of standards, which is consistent with previous studies (Alexander et al., 2005; Sofen et al., 2014; Chen et al., 2016). To quantify the uncertainty in each sample, 30 samples were measured in triplicate, 2 samples in quadruplicate, and 2 samples in duplicate depending on the limitation of sample size. In total, 10 filters sampled in non-polluted days (NPD,  $\text{PM}_{2.5} < 75 \mu\text{g m}^{-3}$ ) and 24 filters sampled in polluted days (PD,  $\text{PM}_{2.5} \geq 75 \mu\text{g m}^{-3}$ ) were analysed.

### 2.3 Estimate of the overall rate of heterogeneous sulfate production

Heterogeneous sulfate production ( $P_{\text{het}}$ ) is commonly parameterized in models according to Eq. (1) (Jacob, 2000; Zheng et al., 2015a):

$$P_{\text{het}} = \frac{3600 \times 96}{RT} \left( \frac{R_p}{D_g} + \frac{4}{v\gamma} \right)^{-1} S_p [\text{SO}_2(\text{g})] \quad (1)$$

where  $P_{\text{het}}$  is in unit of  $\mu\text{g m}^{-3} \text{h}^{-1}$ , 3600 is a time conversion factor ( $\text{s h}^{-1}$ ), 96 is the molar mass of  $\text{SO}_4^{2-}$  ( $\text{g mol}^{-1}$ ),  $R$  is the gas constant ( $0.082 \text{ atm L K}^{-1} \text{ mol}^{-1}$ ), and  $T$  is temperature in K.  $R_p$  is the radius of aerosol particles (m),  $D_g$  is the gas-phase molecular diffusion coefficient of  $\text{SO}_2$  ( $\text{m}^2 \text{s}^{-1}$ ),  $v$  is the mean molecular speed of  $\text{SO}_2$  (g) ( $\text{m s}^{-1}$ ),  $\gamma$  is the uptake coefficient of  $\text{SO}_2$  on aerosols (unitless),  $[\text{SO}_2(\text{g})]$  is the gas-phase concentration of  $\text{SO}_2$  (ppb) and  $S_p$  is the aerosol surface area per unit volume of air ( $\text{m}^2 \text{m}^{-3}$ ). The typical tropospheric value of  $D_g$  and  $v$  is  $2 \times 10^{-5} \text{ m}^2 \text{s}^{-1}$  and  $300 \text{ m s}^{-1}$ , respectively (Jacob, 2000). Observations of  $\text{PM}_{2.5}$  mass concentrations ( $\mu\text{g m}^{-3}$ ) and  $\text{PM}_{2.5}$  mean radius (m) during Beijing haze roughly follows an empirical formula:  $R_p = (0.254 \times \text{PM}_{2.5} + 10.259) \times 10^{-9}$  (Guo et al., 2014). By using the volume and surface area formulas of a sphere and the mean density of particles ( $\rho = 1.5 \times 10^6 \text{ g m}^{-3}$  (Guo et al., 2014)),  $S_p$  can be estimated from Eq. (2). A RH-dependent  $\gamma$  ( $= (2-5) \times 10^{-5}$ , Eq. (3)) derived from Zheng et al. (2015a) during 2013 Beijing haze was used. This range of  $\gamma$  is also consistent with the estimated values of  $\gamma$  from  $(1.6 \pm 0.7)$  to  $(4.5 \pm 1.1) \times 10^{-5}$  by Wang et al. (2016).

$$S_p = \frac{\text{PM}_{2.5} \times 10^{-6}}{4/3 \times \pi R_p^3 \times \rho} \times 4\pi R_p^2 \quad (2)$$

$$\gamma = \begin{cases} 2 \times 10^{-5}, \text{RH} \leq 50 \% \\ 2 \times 10^{-5} + \frac{5 \times 10^{-5} - 2 \times 10^{-5}}{100 - 50} \times (\text{RH} - 50), 50 \% \leq \text{RH} \leq 100 \% \end{cases} \quad (3)$$

### 2.4 Estimate of primary sulfate

The primary sulfate, which is directly emitted into air, includes the sea salt source, terrigenous source and anthropogenic source (Li et al., 2013; Faloona, 2009). The concentration of sea salt sulfate was calculated by using the observed concentrations of  $\text{SO}_4^{2-}$  and  $\text{Na}^+$  and the mass ratio of  $(\text{SO}_4^{2-}/\text{Na}^+) = 0.252$  in seawater (Calhoun et al., 1991). The terrigenous sulfate was estimated using the observed concentrations of  $\text{SO}_4^{2-}$  and  $\text{Ca}^{2+}$  and the mass ratio of  $(\text{SO}_4^{2-}/\text{Ca}^{2+}) = 0.18$  in soil (Legrand et al., 1997), where  $(\text{Ca}^{2+}/\text{Na}^+) = 0.038$  in seawater was used to calculate the fraction of observed  $\text{Ca}^{2+}$  from soil (Legrand and Mayewski, 1997). The anthropogenic primary sulfate is estimated as 3 % of anthropogenic  $\text{SO}_2$  emissions in models (Faloona, 2009; Alexander et al., 2009). Supposing all the observed concentrations of  $\text{SO}_2$  and precursors of secondary sulfate are anthropogenic, we have  $n_{\text{ap}} = 3\% \times (n_{\text{SO}_2} + n_{\text{sas}})$ , where  $n_{\text{sas}} = n_{\text{tos}} - n_{\text{ss}} - n_{\text{ts}} - n_{\text{ap}}$  and  $n_{\text{ap}}$ ,  $n_{\text{sas}}$ ,  $n_{\text{tos}}$ ,  $n_{\text{ss}}$  and  $n_{\text{ts}}$  is the molar concentrations of anthropogenic primary sulfate (ap), secondary sulfate (sas), total sulfate (tos), sea salt sulfate (ss) and terrigenous sulfate (ts). The estimated concentration of total primary sulfate is the sum of primary sulfate from all these sources.

## 2.5 Estimate of sulfate production rate from OH oxidation in the gas-phase

The sulfate production rate from OH oxidation in the gas-phase ( $P_{\text{SO}_2+\text{OH}}$ ) can be expressed as:

$$P_{\text{SO}_2+\text{OH}} = \frac{3600 \times 96 \times R_{\text{SO}_2+\text{OH}}}{RT} \quad (4)$$

where  $P_{\text{SO}_2+\text{OH}}$  is in unit of  $\mu\text{g m}^{-3} \text{h}^{-1}$ , 3600, 96,  $R$  and  $T$  is the same as Eq. (1).  $R_{\text{SO}_2+\text{OH}}$  is the chemical reaction rate ( $\text{ppb s}^{-1}$ ), calculated as shown in Table S1 and S2.

## 2.6 Estimate of in-cloud sulfate production rate

The main in-cloud sulfate formation pathways considered here include S(IV) oxidation by  $\text{H}_2\text{O}_2$ ,  $\text{O}_3$ ,  $\text{NO}_2$  (Wang et al., 2016) and  $\text{O}_2$  via a radical chain mechanism initiated by TMIs (Alexander et al., 2009). Their chemical reaction rate expressions ( $R_{\text{S(IV)+oxi}}$ ) and rate constants ( $k$ ) are summarized in Table S3. The rate of in-cloud sulfate production by a certain oxidant ( $P_{\text{cloud, S(IV)+oxi}}$ ) can be expressed as (Seinfeld and Pandis, 2012):

$$P_{\text{cloud, S(IV)+oxi}} = 3600 \times 96 \times \text{LWC} \times R_{\text{S(IV)+oxi}} \quad (5)$$

where  $P_{\text{cloud, S(IV)+oxi}}$  is in unit of  $\mu\text{g m}^{-3} \text{h}^{-1}$ , 3600 and 96 is the same as Eq. (1), and  $R_{\text{S(IV)+oxi}}$  is in unit of  $\text{M s}^{-1}$ . Cloud liquid water content (LWC, in unit of  $\text{mg m}^{-3}$ ) was derived from a global reanalysis, GEOS-FP (<https://gmao.gsfc.nasa.gov/products/>).

## 2.7 Isotopic constraints on sulfate formation pathways

Since S(IV) oxidation by  $\text{O}_3$  and  $\text{H}_2\text{O}_2$  are the sole sources of non-zero  $\Delta^{17}\text{O}(\text{SO}_4^{2-})$  (Table 1) (Savarino et al., 2000), the relative importance of different sulfate formation pathways can be calculated as follows (Alexander et al., 2012):

$$\Delta^{17}\text{O}_{\text{obs}} = (6.5 \times f_{\text{S(IV)+O}_3}) + (0.7 \times f_{\text{S(IV)+H}_2\text{O}_2}) + (0 \times f_{\text{zero-}\Delta^{17}\text{O}}) \quad (6)$$

where  $f_{\text{S(IV)+O}_3}$  and  $f_{\text{S(IV)+H}_2\text{O}_2}$  are the fractional contributions of S(IV) oxidation by  $\text{O}_3$  and  $\text{H}_2\text{O}_2$  oxidation to total sulfate production, respectively, and  $f_{\text{zero-}\Delta^{17}\text{O}}$  represents the fractional contribution of sulfate with zero- $\Delta^{17}\text{O}$  processes such as primary sulfate, secondary sulfate formed via OH oxidation,  $\text{NO}_2$  oxidation, and  $\text{O}_2$  oxidation. By definition, we have  $f_{\text{S(IV)+O}_3} + f_{\text{S(IV)+H}_2\text{O}_2} + f_{\text{zero-}\Delta^{17}\text{O}} = 100\%$ .

In addition, as sulfate with non-zero  $\Delta^{17}\text{O}(\text{SO}_4^{2-})$  is produced either via in-cloud reactions or via heterogeneous reactions or both, Eq. (6) can also be written as follows:

$$\Delta^{17}\text{O}_{\text{obs}} = f_{\text{het}} \times \Delta^{17}\text{O}_{\text{het}} + f_{\text{cloud}} \times \Delta^{17}\text{O}_{\text{cloud}} + f_{\text{SO}_2+\text{OH}} \times \Delta^{17}\text{O}_{\text{SO}_2+\text{OH}} + f_{\text{p}} \times \Delta^{17}\text{O}_{\text{p}} \quad (7)$$

where  $f_{\text{het}}$ ,  $f_{\text{cloud}}$ ,  $f_{\text{SO}_2+\text{OH}}$  and  $f_{\text{p}}$  respectively represents the fractional contribution of heterogeneous sulfate production, in-cloud sulfate production, gas-phase sulfate production and primary sulfate to the observed sulfate.  $\Delta^{17}\text{O}_{\text{het}}$ ,  $\Delta^{17}\text{O}_{\text{cloud}}$ ,  $\Delta^{17}\text{O}_{\text{SO}_2+\text{OH}}$  and  $\Delta^{17}\text{O}_{\text{p}}$  respectively represents  $\Delta^{17}\text{O}$  of corresponding sulfate produced via above pathways. Both  $\Delta^{17}\text{O}_{\text{SO}_2+\text{OH}}$  and  $\Delta^{17}\text{O}_{\text{p}}$  are

equal to 0 ‰.  $\Delta^{17}\text{O}_{\text{cloud}}$  can be calculated as shown in Eq. (8) as the lifetime of sulfate produced in clouds will not depend on the specific S(IV) oxidant.

$$\Delta^{17}\text{O}_{\text{cloud}} = \frac{6.5 \times P_{\text{cloud}, \text{S(IV)} + \text{O}_3} + 0.7 \times P_{\text{cloud}, \text{S(IV)} + \text{H}_2\text{O}_2}}{P_{\text{cloud}}} \quad (8)$$

where  $P_{\text{cloud}}$  is the rate of total in-cloud sulfate production, which was calculated as the sum of in-cloud S(IV) oxidation by  $\text{H}_2\text{O}_2$ ,  $\text{O}_3$ ,  $\text{NO}_2$  and  $\text{O}_2$  initiated by TMIs.

## 2.8 Calculation of aerosol water content (AWC), aerosol pH and ionic strength ( $I_s$ )

AWC, aerosol pH and  $I_s$  was calculated by the ISORROPIA II model, which is a thermodynamic equilibrium model for  $\text{NH}_4^+ - \text{K}^+ - \text{Ca}^{2+} - \text{Na}^+ - \text{Mg}^{2+} - \text{SO}_4^{2-} - \text{NO}_3^- - \text{Cl}^- - \text{H}_2\text{O}$  aerosols (Fountoukis and Nenes, 2007). The ISORROPIA II model can solve forward problems in which  $T$ , RH and the concentrations of gas + aerosols are known (e.g.,  $\text{NH}_3 + \text{NH}_4^+$ ), and reverse problems in which  $T$ , RH and the concentrations of aerosol (but not gas) species are known. We used the forward method to calculate AWC, aerosol pH and  $I_s$  as this method has been shown to best predict aerosol pH (Hennigan et al., 2015). The AWC, pH and  $I_s$  was first calculated in metastable mode (assuming that bulk aerosol solution is supersaturated), which is consistent with previous studies about Beijing haze (Liu et al., 2017; Guo et al., 2017). However, the work of Rood et al. (1989) in California, USA suggested that not all aerosols are in metastable state, even though the fractional occurrence of metastable aerosols increases with increasing RH in urban sites (i.e., from near 0 at RH < round 30 % to near 100 % at RH > round 80 %, roughly following Eq. (9)). We also calculated the AWC, pH and  $I_s$  assuming stable mode (assuming that bulk aerosols crystallize once saturation is exceeded), which is consistent with Wang et al. (2016). The input of observed inorganic ion concentrations and meteorological parameters are summarized in Table S4. Since gaseous  $\text{NH}_3$  was not measured in our campaign, we used the empirical equation  $\text{NH}_3 \text{ (ppb)} = 0.34 \times \text{NO}_x \text{ (ppb)} + 0.63$ , derived from observations of Meng et al. (2011) in Beijing winter, to estimate the  $\text{NH}_3$  concentrations. We used  $\text{NO}_2$  concentrations instead of  $\text{NO}_x$  as input due to the lack of  $\text{NO}_x$  observations in our study, which would give a lower end of the  $\text{NH}_3$  concentrations. Given the importance of AWC for reaction rates and the fact that ISORROPIA II underestimates AWC at low RH (Bian et al., 2014), samples with RH < 40 % are excluded from analysis (Hennigan et al., 2015). This excludes 8 out of the total 34 samples (24 %), with 6 of them in NPD. A total of 4 samples in NPD and 22 samples in PD were analysed for AWC, aerosol pH and  $I_s$  using observations and the ISORROPIA II model. Due to that the predicted  $I_s$  is high ( $I_s > 10 \text{ M}$ , Table S4), which suggests aerosol water is non-ideal, the influence of  $I_s$  on reaction rate constants (Table S3) and effective Henry's law constants (Table S5) is taken into consideration when the influence is known.

$$\text{MF} = \begin{cases} 0, & \text{RH} < 30 \% \\ -0.024 \times \text{RH}^2 + 4.18 \times \text{RH} - 89.13, & 30 \% \leq \text{RH} \leq 80 \% \\ 100 \%, & 80 \% < \text{RH} \leq 100 \% \end{cases} \quad (9)$$

where MF (in %) is the fraction of metastable aerosols to total aerosols.



## 2.9 Estimate of aqueous concentrations of trace species

The aqueous concentrations of SO<sub>2</sub>, O<sub>3</sub>, H<sub>2</sub>O<sub>2</sub> and NO<sub>2</sub> were calculated as described in Table S5. The determination of in-cloud concentrations of TMIs (here only Fe(III) and Mn(II) (Alexander et al., 2009)) is described below.

The concentration of soluble Fe(III) follows Eqs. (10)–(13) (Liu and Millero, 1999):

$$\log_{10}[\text{Fe(III)}] = \log_{10} K_{\text{Fe(OH)}_3}^* + 3 \times \log_{10}[\text{H}^+] + \log_{10}(1 + \beta_1^*[\text{H}^+]^{-1} + \beta_2^*[\text{H}^+]^{-2}) \quad (10)$$

where

$$\log_{10} K_{\text{Fe(OH)}_3}^* = -13.486 - 0.1856 \times I_s^{0.5} + 0.3073 \times I_s + 5254/T \quad (11)$$

$$\log_{10} \beta_1^* = 2.517 - 0.8885 \times I_s^{0.5} + 0.2139 \times I_s - 1320/T \quad (12)$$

$$\log_{10} \beta_2^* = 0.4511 - 0.3305 \times I_s^{0.5} - 1996/T \quad (13)$$

and [Fe(III)] is the aqueous concentration of Fe(III) in unit of M,  $T$  is temperature in unit of K, and  $I_s$  is ionic strength in unit of M,  $K_{\text{Fe(OH)}_3}^*$  is the solubility product constant of Fe(OH)<sub>3</sub>, and  $\beta_1^*$  and  $\beta_2^*$  is respectively first-order and second-order cumulative hydrolysis constants of Fe<sup>3+</sup>.

Our calculation suggested in-cloud [Fe(III)] was in the range of 0.6 to 6.1 μM with a mean of (2.6±1.8) μM, which is similar to the observed values in NCP (Guo et al., 2012; Shen et al., 2012). The concentration of soluble Mn(II) in cloud water was set to be 1 μM in the present study, which is the general value observed in cloud water in NCP (Guo et al., 2012; Shen et al., 2012).

## 2.10 Estimate of sulfate production rate in aerosol water

The reaction rate expressions, rate constants ( $k$ ) and the influence of  $I_s$  on  $k$  for sulfate production in aerosol water are summarized in Table S3. The overall rates for S(IV) oxidation in aerosol water depend not only on chemical reaction rates (Table S3) but also on mass transport limitations. A standard resistance model was used to estimate effects of mass transport following the work of Cheng et al. (2016):

$$\frac{1}{R_{\text{H,S(IV)+oxi}}} = \frac{1}{R_{\text{S(IV)+oxi}}} + \frac{1}{J_{\text{aq,lim}}} \quad (14)$$

where  $R_{\text{H,S(IV)+oxi}}$  is the overall reaction rate for S(IV) oxidation by a certain oxidant (oxi) such as O<sub>3</sub>, H<sub>2</sub>O<sub>2</sub>, NO<sub>2</sub> and O<sub>2</sub> on acidic microdroplets (M s<sup>-1</sup>),  $R_{\text{S(IV)+oxi}}$  is the chemical reaction rate (M s<sup>-1</sup>) and  $J_{\text{aq,lim}}$  is the rate limited by mass transfer from the gas to the aqueous phase (M s<sup>-1</sup>). Due to the large decrease in the aqueous-phase reaction rate constant for TMI-initiated S(IV) oxidation by O<sub>2</sub> with increasing  $I_s$  (Martin and Hill, 1967) and the high  $I_s$  of aerosols (Table S4), combined with the fact that the rate constant for the S(IV) + O<sub>2</sub> mechanism on acidic microdroplets proposed by Hung and Hoffman (2015) likely includes the effect of TMIs, we do not directly consider TMI-initiated S(IV) oxidation by O<sub>2</sub> in aerosol water.  $R_{\text{S(IV)+oxi}}$  was calculated as described in Table S3. The limiting mass transfer  $J_{\text{aq,lim}}$  was calculated by Eqs. (15) and (16).

$$J_{\text{aq,lim}} = \min\{J_{\text{aq}}(\text{SO}_2), J_{\text{aq}}(\text{oxi})\} \quad (15)$$



$$J_{\text{aq}}(X) = k_{\text{MT}}(X) \times [X(\text{aq})] \quad (16)$$

where  $X = \text{SO}_2, \text{O}_3, \text{H}_2\text{O}_2$  or  $\text{NO}_2$  and  $k_{\text{MT}} (\text{s}^{-1})$  is the mass transfer rate coefficient and was calculated as Eq. (17) (Cheng et al., 2016; Seinfeld and Pandis, 2012):

$$k_{\text{MT}}(X) = \left[ \frac{R_p^2}{3D_g} + \frac{4R_p}{3\alpha v} \right]^{-1} \quad (17)$$

where  $R_p$ ,  $D_g$  and  $v$  are the same as Eq. (1). The  $\alpha$  used in our calculation is respectively 0.11 for  $\text{SO}_2$ , 0.23 for  $\text{H}_2\text{O}_2$ ,  $2.0 \times 10^{-3}$  for  $\text{O}_3$  and  $2.0 \times 10^{-4}$  for  $\text{NO}_2$  (Seinfeld and Pandis, 2012; Jacob, 2000). The term on the left hand side of Eq. (17) is the gas-phase diffusion limitation while the term on the right hand side of Eq. (17) is the interfacial mass transport limitation.  $k_{\text{MT}}$  was limited by interfacial mass transport in our study.

The rate of heterogeneous sulfate production by a certain oxidant ( $P_{\text{het, S(IV)+oxi}}$ ) in aerosol water can be expressed as:

$$P_{\text{het, S(IV)+oxi}} = 3600 \times 96 \times \text{AWC} \times R_{\text{H, S(IV)+oxi}} \quad (18)$$

where  $P_{\text{het, S(IV)+oxi}}$  is in the unit of  $\mu\text{g m}^{-3} \text{h}^{-1}$ , 3600 and 96 is the same as Eq. (1). AWC is in the unit of  $\text{mg m}^{-3}$  and  $R_{\text{H, S(IV)+oxi}}$  is in the unit of  $\text{M s}^{-1}$ .

## 3 Results and Discussion

### 3.1 Characteristics of haze events in Beijing

Figure 1a shows the temporal evolution of concentrations of  $\text{PM}_{2.5}$  and  $\text{SO}_4^{2-}$  during our sampling period. The 12h-averaged  $\text{PM}_{2.5}$  concentrations ranged from 16 to  $323 \mu\text{g m}^{-3}$  with a mean of  $(141 \pm 88 (1\sigma)) \mu\text{g m}^{-3}$ . In comparison, the Grade II of the Chinese National Ambient Air Quality Standard of daily  $\text{PM}_{2.5}$  is  $75 \mu\text{g m}^{-3}$ . The  $\text{SO}_4^{2-}$  concentrations varied from 1.5 to  $56.4 \mu\text{g m}^{-3}$  with a mean of  $(21.2 \pm 15.4) \mu\text{g m}^{-3}$ . As shown in Fig. 1a,  $\text{SO}_4^{2-}$  concentrations presented a similar temporal trend as  $\text{PM}_{2.5}$  concentrations, i.e., increased from a mean of  $(3.9 \pm 1.8) \mu\text{g m}^{-3}$  in non-polluted days (NPD,  $\text{PM}_{2.5} < 75 \mu\text{g m}^{-3}$ ) to  $(28.4 \pm 12.5) \mu\text{g m}^{-3}$  in polluted days (PD,  $\text{PM}_{2.5} \geq 75 \mu\text{g m}^{-3}$ ). The fraction of  $\text{SO}_4^{2-}$  to  $\text{PM}_{2.5}$  mass concentration ranged from 8–25 %, and increased from a mean of  $(11 \pm 2) \%$  in NPD to  $(15 \pm 5) \%$  in PD. The sulfur oxidation ratio ( $\text{SOR} = n\text{SO}_4^{2-}/(n\text{SO}_4^{2-} + n\text{SO}_2)$ , where  $n\text{SO}_4^{2-}$  and  $n\text{SO}_2$  represents the molar concentration of  $\text{SO}_4^{2-}$  and  $\text{SO}_2$ , respectively), a proxy for secondary sulfate formation (Sun et al., 2006), also increased rapidly with  $\text{PM}_{2.5}$  levels, from a mean of  $(0.12 \pm 0.04)$  in NPD to  $(0.41 \pm 0.17)$  in PD (Fig. 1b).

Observed  $\Delta^{17}\text{O}(\text{SO}_4^{2-})$  ( $\Delta^{17}\text{O}_{\text{obs}}$ ) ranged from 0.1 ‰ to 1.6 ‰ with a mean of  $(0.9 \pm 0.3) \%$  (Fig. 1b). The highest  $\Delta^{17}\text{O}_{\text{obs}} = 1.6 \%$  occurred during PD of Case II in October 2014 while the lowest  $\Delta^{17}\text{O}_{\text{obs}} = 0.1 \%$  occurred during PD of Case IV in December 2014.  $\Delta^{17}\text{O}_{\text{obs}}$  reported here is similar in magnitude to previous observations of  $\Delta^{17}\text{O}(\text{SO}_4^{2-})$  in aerosols and rainwater collected in China (Lin et al., 2017; Li et al., 2013) and other mid-latitude sites (Table S6). The overall  $\Delta^{17}\text{O}_{\text{obs}}$  levels during our entire sampling time are similar for NPD and PD, being  $(0.9 \pm 0.1) \%$  and  $(0.9 \pm 0.4) \%$ , respectively. However, the NPD to PD difference of  $\Delta^{17}\text{O}_{\text{obs}}$  can be case-dependent. For Case I and II in October 2014,  $\Delta^{17}\text{O}_{\text{obs}}$  increased from NPD to PD,

while the opposite trend was observed for Case III to V in November 2014 to January 2015 (Fig. 1b). These  $\Delta^{17}\text{O}_{\text{obs}}$  variations are generally similar to variability in concentrations of observed  $\text{O}_3$  and calculated  $\text{H}_2\text{O}_2$  (Fig. 1c), which is consistent with the fact that  $\text{O}_3$  and  $\text{H}_2\text{O}_2$  are the sole sources of non-zero  $\Delta^{17}\text{O}(\text{SO}_4^{2-})$  (Table 1).

### 3.2 Direct estimate of sulfate formation pathways based on $\Delta^{17}\text{O}_{\text{obs}}$

Figure 2 shows the calculated possible fractional contributions of each formation pathway ( $f_{\text{S(IV)}+\text{H}_2\text{O}_2}$ ,  $f_{\text{S(IV)}+\text{O}_3}$ , and  $f_{\text{zero-}\Delta^{17}\text{O}}$ ) for each sample using Eq. (6). On average over all samples collected,  $f_{\text{S(IV)}+\text{O}_3} = 4\text{--}13\%$ ,  $f_{\text{S(IV)}+\text{H}_2\text{O}_2} = 0\text{--}88\%$ , and  $f_{\text{zero-}\Delta^{17}\text{O}} = 8\text{--}87\%$ . For samples during PD of Case IV in December 2014 with the three lowest  $\Delta^{17}\text{O}_{\text{obs}}$  values (Fig. 1b),  $f_{\text{zero-}\Delta^{17}\text{O}}$  was respectively in the range of 57–95 %, 86–98 % and 57–95 %, corresponding to  $f_{\text{S(IV)}+\text{H}_2\text{O}_2}$  being in the range of 0–43 %, 0–14 % and 0–43 % respectively, which clearly suggests zero- $\Delta^{17}\text{O}$  pathways dominated sulfate formation during PD of Case IV. However, for other samples, the maximum possible  $f_{\text{S(IV)}+\text{H}_2\text{O}_2}$  ranged from 71 to 100 % with a mean of  $(93 \pm 7)\%$  while the maximum possible  $f_{\text{zero-}\Delta^{17}\text{O}}$  was 75 to 92 % with a mean of  $(86 \pm 4)\%$ , implying that sulfate formation during these sampling periods were dominated by  $\text{H}_2\text{O}_2$  oxidation and/or zero- $\Delta^{17}\text{O}$  pathways.

### 3.3 Chemical kinetic calculations with the constraint of $\Delta^{17}\text{O}_{\text{obs}}$

The good correlation between RH and SOR in Fig. 3a ( $r = 0.76$ ,  $p < 0.01$ ) suggests heterogeneous reactions played an important role in sulfate formation. Our calculations show that overall heterogeneous sulfate production ( $P_{\text{het}}$ , see Sect. 2.3) presented similar trends with  $\text{SO}_4^{2-}$  concentrations except for Case II (Fig. 3b) and increased from a mean of  $(0.6 \pm 0.3) \mu\text{g m}^{-3} \text{h}^{-1}$  in NPD to  $(2.0 \pm 1.1) \mu\text{g m}^{-3} \text{h}^{-1}$  in PD during our entire sampling period. In comparison, Cheng et al. (2016) reported that the missing sulfate production rate required to explain the observed sulfate concentration is around  $0.07 \mu\text{g m}^{-3} \text{h}^{-1}$  when  $\text{PM}_{2.5} < 50 \mu\text{g m}^{-3}$  and around  $4 \mu\text{g m}^{-3} \text{h}^{-1}$  when  $\text{PM}_{2.5} > 400 \mu\text{g m}^{-3}$  during 2013 Beijing haze. We also calculated the contribution from primary sulfate and performed chemical kinetic calculations including  $\text{SO}_2$  oxidation by OH in the gas-phase and in-cloud sulfate production (Fig. 4 and Table S7, see Sect. 2.4–2.6) to estimate the relative importance of heterogeneous sulfate production in our sampling period. Heterogeneous reactions were found to dominate sulfate formation during PD in four out of the total five cases (except for Case II) with fractional contributions of 42 to 54 % and a mean of  $(48 \pm 5)\%$  (Fig. 4). This is consistent with Zheng et al. (2015a) who modelled that about half of the observed sulfate was from heterogeneous reactions during 2013 Beijing haze. In contrast, we found that during PD of Case II in October 2014, heterogeneous sulfate production only accounted for 23 % of total sulfate production while in-cloud sulfate production predominated total sulfate production with an estimated fraction of 68 %. The predominant role of in-cloud sulfate production in PD of Case II was supported by the relative high LWC during this time period (Fig. 5a). Our calculations also suggest the in-cloud sulfate production was dominated by  $\text{H}_2\text{O}_2$  oxidation throughout our sampling period (Fig. 5b), which is consistent with previous findings that  $\text{H}_2\text{O}_2$  oxidation is the most important in-cloud sulfate production pathway globally (Alexander et al., 2012) and in

NCP (Shen et al., 2012). In addition, the  $\Delta^{17}\text{O}$  of sulfate produced in clouds ( $\Delta^{17}\text{O}_{\text{cloud}}$ ) was estimated to range from 0.5 ‰ to 0.8 ‰ with a mean of  $(0.6 \pm 0.1)$  ‰ during our sampling period and showed similar variations with  $\Delta^{17}\text{O}_{\text{obs}}$  (Fig. 5c). The mean value of  $\Delta^{17}\text{O}_{\text{cloud}}$  calculated here is close to  $\Delta^{17}\text{O}(\text{SO}_4^{2-})$  in rainwater observed in central China ( $0.53 \pm 0.19$  ‰) (Li et al., 2013) and at Baton Rouge, USA ( $0.62 \pm 0.32$  ‰) (Jenkins and Bao, 2006). In addition, by using Eq. (7), the  $\Delta^{17}\text{O}$  of sulfate produced via heterogeneous reactions ( $\Delta^{17}\text{O}_{\text{het}}$ ) was calculated to range from 0.1 ‰ to 3.1 ‰ in our study.

To explore the specific mechanisms of heterogeneous oxidation of  $\text{SO}_2$ , we calculated aerosol parameters such as aerosol water content (AWC), pH and ionic strength ( $I_s$ ) by using the ISORROPIA II thermodynamic model (Fountoukis and Nenes, 2007) (Fig.6, see Sect. 2.8). It was found that the assumptions about aerosol thermodynamic state (salts crystallize once saturation is exceeded, termed as “stable state” or aerosol solution is supersaturated, termed as “metastable state”) significantly influence the calculated aerosol pH, but have little impact on the calculated AWC and  $I_s$  (Fig. 6). Calculated AWC increased with  $\text{PM}_{2.5}$  concentrations, from  $(5.3 \pm 7.4)$   $\mu\text{g m}^{-3}$  in NPD to  $(63.5 \pm 54.6)$   $\mu\text{g m}^{-3}$  in PD when assuming stable state and from  $(9.6 \pm 6.0)$   $\mu\text{g m}^{-3}$  in NPD to  $(84.2 \pm 49.2)$   $\mu\text{g m}^{-3}$  in PD when assuming metastable state (Fig. 6a). Calculated  $I_s$  was similar for stable and metastable assumptions, ranging from 11.3 to 51.6 M (Fig. 6b). The high  $I_s$  suggested aerosol water was non-ideal and thus the influence of  $I_s$  on reaction rate constants (Table S3) and effective Henry’s law constants (Table S5) was taken into consideration when the influence is known. The bulk aerosol pH predicted in stable state was in the range of 7.5 to 7.8 with a mean of  $(7.6 \pm 0.1)$ , consistent with bulk aerosol pH  $(7.63 \pm 0.03)$  calculations during a haze event in Beijing 2015 predicted by Wang et al. (2016). The bulk aerosol pH calculated assuming metastable state was in the range of 3.4 to 7.6 with a mean of  $(4.7 \pm 1.1)$ , consistent with the mean value of 4.2 calculated in metastable aerosol assumption during severe haze in Beijing 2015–2016 by Liu et al. (2017). The calculated aerosol pH assuming metastable state decreased with increasing  $\text{PM}_{2.5}$  levels, from a mean of  $(6.5 \pm 1.3)$  in NPD to  $(4.4 \pm 0.6)$  in PD, while that assuming stable state shows no relationship with  $\text{PM}_{2.5}$  concentrations (Fig. 6c). Our measured pH of filtrate ranged from 4.6 to 8.2 with a mean of  $(5.7 \pm 1.0)$ , similar to pH of filtrate from  $\text{PM}_{2.5}$  in Beijing reported by Wang et al. (2005). The measured pH of filtrate shows similar trends with bulk aerosol pH calculated assuming metastable state (Fig. 6c), with a mean value  $(6.9 \pm 0.7)$  in NPD and  $(5.1 \pm 0.6)$  in PD, which suggests that bulk aerosols are in metastable state with moderate acidity in PD. This is also consistent with our estimate that most aerosols are in metastable with a fraction of  $(74 \pm 17)$  % in PD by using Eq. (9) and our cognition that the mixture of major acidic aerosols with minor neutral aerosols would lead to the bulk being acidic. However, as the effective Henry’s law constant of  $\text{SO}_2$  at pH = 7.6 (stable state) can be 3 orders magnitude higher than that at pH = 4.4 (metastable state in PD) rendering even a small fraction of aerosol at this high pH value being potentially significant active sites for heterogeneous sulfate production during PD.

The main heterogeneous sulfate formation pathways considered include S(IV) oxidation by  $\text{H}_2\text{O}_2$ ,  $\text{O}_3$ ,  $\text{NO}_2$  and  $\text{O}_2$  on acidic microdroplets as proposed by Hung and Hoffmann (2015). Other sulfate formation pathways such as S(IV) oxidation by

NO<sub>3</sub> radical, methyl-hydrogenperoxide (MHP), peroxyacetic acid (PAA), and hypohalous acids in aerosol water (Feingold et al., 2002; Walcek and Taylor, 1986; Chen et al., 2017) is thought to be negligible during haze in NCP (Cheng et al., 2016), and thus is not considered here. We estimate the relative importance of these heterogeneous sulfate formation pathways as follows. First, the heterogeneous sulfate production rate via S(IV) oxidation by H<sub>2</sub>O<sub>2</sub> ( $P_{\text{het, S(IV)+H}_2\text{O}_2}$ ) was calculated with the influence of  $I_s$  being considered, which has been determined at high  $I_s$  in laboratories (Table S3 and S5). Then, the fractional contribution of H<sub>2</sub>O<sub>2</sub> oxidation ( $f_{\text{het, S(IV)+H}_2\text{O}_2}$ ) to overall heterogeneous sulfate production ( $P_{\text{het}}$ ) calculated using apparent  $\gamma$  (see Sect. 2.3) was estimated. Large uncertainties exist in the influence of  $I_s$  on the reaction rate constant of S(IV) oxidation by O<sub>3</sub> in aerosol water (Table S3), renders the estimate of its fractional contribution ( $f_{\text{het, S(IV)+O}_3}$ ) to  $P_{\text{het}}$  from purely chemical kinetic calculations uncertain. Instead,  $f_{\text{het, S(IV)+O}_3}$  was estimated using our calculated  $f_{\text{het, S(IV)+H}_2\text{O}_2}$  and  $\Delta^{17}\text{O}_{\text{het}}$  values, on the basis that  $\Delta^{17}\text{O}(\text{SO}_4^{2-}) > 0$  ‰ originates solely from H<sub>2</sub>O<sub>2</sub> and O<sub>3</sub> oxidation. Then zero- $\Delta^{17}\text{O}$  pathways such as S(IV) oxidation by NO<sub>2</sub> and by O<sub>2</sub> was estimated to be the remaining part ( $f_{\text{het, zero-}\Delta^{17}\text{O}}$ ). At last, the potential importance of S(IV) oxidation by NO<sub>2</sub> and by O<sub>2</sub> is discussed.

Calculations show that  $f_{\text{het, S(IV)+H}_2\text{O}_2}$  was 4–6 % with a mean of (5 ± 1) % under stable aerosol assumptions, and 8–19 % with a mean of (13 ± 4) % under metastable state assumptions for PD of all the cases.  $f_{\text{het, S(IV)+O}_3}$  was calculated to be 2–47 % with a mean of (22 ± 17) % in stable state assumption and 0–47 % with a mean of (21 ± 18) % in metastable state assumption. Correspondingly,  $f_{\text{het, zero-}\Delta^{17}\text{O}}$  was the remaining 73 % (47–94 %) in stable assumption, or 66 % (42–81 %) in metastable assumption for PD of all the cases (Fig. 7). Excluding PD of Case II, in which sulfate formation was predominated by in-cloud reactions, our calculations suggest zero- $\Delta^{17}\text{O}$  pathways such as S(IV) oxidation by NO<sub>2</sub> and/or by O<sub>2</sub> are important for sulfate formation during Beijing haze.

Cheng et al. (2016) suggested that S(IV) oxidation by NO<sub>2</sub> in aerosol water could largely account for the missing sulfate source in 2013 Beijing haze. In their study, the calculated mean aerosol pH is 5.8, while influence of  $I_s$  was not taken into account due to the lack of relevant experimental data. The calculated  $P_{\text{het, S(IV)+NO}_2}$  is highly sensitive to aerosol pH. In our study, when aerosol pH decreased from (7.6 ± 0.1) assuming stable state to (4.7 ± 1.1) assuming metastable state, mean  $P_{\text{het, S(IV)+NO}_2}$  decreased from (6.5 ± 7.7) μg m<sup>-3</sup> h<sup>-1</sup> to (0.01 ± 0.02) μg m<sup>-3</sup> h<sup>-1</sup> for PD of all the cases (Fig. 7). The former is much larger than our estimate of overall heterogeneous production rate,  $P_{\text{het}} = (2.0 \pm 1.1)$  μg m<sup>-3</sup> h<sup>-1</sup>, while the latter is too small. Moreover, the influence of  $I_s$  was not considered, which is expected to increase the reaction rate constant of S(IV) oxidation by NO<sub>2</sub> (Cheng et al., 2016). The treatment of aerosols as a bulk quantity, assuming that all aerosols are either in stable or metastable state, or that all aerosol particles have the same pH, may lead to errors in calculating heterogeneous sulfate production rates. As stated in Sect. 2.8, not all aerosols are in metastable state, even though the fractional occurrence of metastable aerosols increases with increasing RH (Rood et al., 1989). Fig. 8a shows that the fraction of metastable aerosols to total aerosols (MF in %), estimated by using Eq. (9), increases with PM<sub>2.5</sub> levels. However, when assuming a combination of stable and metastable state aerosol as

shown in Eq. (9),  $P_{\text{het, S(IV)+NO}_2}$  increases with  $\text{PM}_{2.5}$  levels and reaches  $(0.9 \pm 0.7) \mu\text{g m}^{-3} \text{h}^{-1}$  during PD of all the cases (Fig. 8b), much higher than  $P_{\text{het, S(IV)+NO}_2} = (0.01 \pm 0.02) \mu\text{g m}^{-3} \text{h}^{-1}$  under sole metastable aerosol assumption. This estimate suggests that even though the majority of aerosols may be in metastable state during PD ( $74 \pm 17\%$  in our calculation), the high pH of the minority of aerosols in stable state could render S(IV) oxidation by  $\text{NO}_2$  a potentially significant pathway for heterogeneous sulfate production.

Since  $P_{\text{het, S(IV)+NO}_2}$  using calculated aerosol pH assuming metastable state was two orders of magnitude lower than  $P_{\text{het}}$  during PD, we further examined S(IV) oxidation by  $\text{O}_2$  on acidic microdroplets under the metastable state assumption. A laboratory study suggested that  $\text{SO}_2$  oxidation by  $\text{O}_2$  on acidic microdroplets has a large aqueous-phase reaction rate constant of  $1.5 \times 10^6 [\text{S(IV)}] (\text{M s}^{-1})$  at  $\text{pH} \leq 3$ , a pH range much lower than our calculated pH values. The rate constant was shown to decrease with increasing pH, however, no values of the rate constant at  $\text{pH} > 3$  was reported (Hung and Hoffmann, 2015). Figure 7b shows heterogeneous sulfate production rate via S(IV) oxidation by  $\text{O}_2$  on acidic microdroplets ( $P_{\text{het, S(IV)+O}_2}$ ) with AWC calculated assuming metastable state and the aqueous-phase rate constant for  $\text{pH} \leq 3$  being used, even though the calculated aerosol pH is  $> 3$ . The estimated  $P_{\text{het, S(IV)+O}_2}$  is  $1.5 \times 10^3$  to  $1.3 \times 10^5 \mu\text{g m}^{-3} \text{h}^{-1}$  with a mean of  $2.5 \times 10^4 \mu\text{g m}^{-3} \text{h}^{-1}$  during PD of all cases, which is four order of magnitude larger than  $P_{\text{het}}$ . This value should be an overestimate due to our calculated bulk aerosol pH predicted in metastable state being  $(4.4 \pm 0.6)$  during PD and the experimental results of He et al. (2014) and Wang et al. (2016) suggests  $\text{O}_2$  oxidation pathway is negligible at higher pH conditions (e.g., on  $\text{CaO}$  and in  $\text{NH}_4^+$  solution). However, some fraction of aerosols may have  $\text{pH} \leq 3$  due to the Kelvin effect (Hung and Hoffmann, 2015), rendering S(IV) oxidation by  $\text{O}_2$  on acidic microdroplets a potentially important pathway for heterogeneous sulfate production even if it may occur on only a small fraction of the ambient aerosol.

#### 4 Conclusions

Our study suggests that both in-cloud reactions and heterogeneous reactions can dominate sulfate formation during Beijing haze, with the fractional contribution of  $f_{\text{cloud}} = 68\%$  in Case II and  $f_{\text{het}} = (48 \pm 5)\%$  in Case I and III–V. The  $\Delta^{17}\text{O}$ -constrained calculation shows that the heterogeneous sulfate production during haze events in our observation was mainly (66 to 73 % on average) from reactions that result in sulfate with  $\Delta^{17}\text{O} = 0\%$ , e.g., S(IV) oxidation by  $\text{NO}_2$  and/or by  $\text{O}_2$ . S(IV) oxidation by  $\text{H}_2\text{O}_2$  and  $\text{O}_3$  accounted for the rest (27 to 34 %) of heterogeneous sulfate production. However, given the large difference in predicted aerosol pH assuming metastable aerosol state and stable aerosol state ( $\text{pH} = 7.6 \pm 0.1$  and  $4.7 \pm 1.1$ , respectively) and the strong dependence of  $\text{SO}_2$  oxidation on aerosol pH, we cannot quantify the relative importance of these two pathways for heterogeneous sulfate production. S(IV) +  $\text{NO}_2$  can be the dominant pathway when aerosols are in stable state with  $\text{pH} = 7.6 \pm 0.1$ , while S(IV) +  $\text{O}_2$  can take over providing that highly acidic aerosols ( $\text{pH} \leq 3$ ) exist. To distinguish

388 which of these two mechanisms is more important for sulfate formation during Beijing haze, the heterogeneity of aerosol state  
389 and pH should be considered in future studies.

## 390 **Supplementary Materials**

391 **Table S1.** Reaction rate expression and constant for SO<sub>2</sub> oxidation by OH in the gas-phase.

392 **Table S2.** The daytime average OH concentration.

393 **Table S3.** Aqueous-phase reaction rate expressions, rate constants (*k*) and influence of ionic strength (*I<sub>s</sub>*) on *k* for sulfate  
394 production in aerosol and cloud water.

395 **Table S4.** The input and output of ISORROPIA II model.

396 **Table S5.** Calculations of aqueous-phase concentrations, equilibrium constants and influence of ionic strength.

397 **Table S6.** Observed Δ<sup>17</sup>O(SO<sub>4</sub><sup>2-</sup>) in aerosols or rainwater in mid-latitude areas.

398 **Table S7.** Estimated fractional contribution of different sulfate production pathways during Beijing haze.

## 399 **Data availability**

400 All data needed to draw the conclusions in the present study are shown in this paper and/or the Supplementary  
401 Materials. For additional data related to this study, please contact the corresponding author ([zqxie@ustc.edu.cn](mailto:zqxie@ustc.edu.cn)).

## 402 **Author contributions**

403 Z.Q.X. initiated and led the study. P.Z.H. conducted oxygen isotope measurements supervised by B.A. and L.G.. P.Z.H.,  
404 X.Y.C, S.D.F., H.C.Z., H. K. performed the field experiments and aerosol chemical composition measurements. P.Z.H., B.A.,  
405 Z.Q.X., L.G., H.S. and Y.F.C. interpreted the data. H.S., Y.F.C. and G.J.Z. involved the discussion of oxidation pathway  
406 calculation. C.L. contributed to the field observation support. P.Z.H. wrote the manuscript with B.A., Z.Q.X. and L.G. inputs.  
407 All authors involved the discussion and revision.

## 408 **Competing interests**

409 The authors declare no competing interests.

## 410 **Acknowledgments**

411 We thank A. J. Schauer and Q. J. Chen at the University of Washington for help with isotope ratio measurements. Z. Q.  
412 Xie acknowledges support from National Key Project of MOST (2016YFC0203302), NSFC (91544013), and the Key Project

of CAS (KJZD-EW-TZ-G06-01). B. Alexander acknowledges support from NSF AGS 1644998. H. Su acknowledges support from National Key Project of MOST (2017YFC0210104) and NSFC (91644218).

## References

- Alexander, B., Park, R. J., Jacob, D. J., Li, Q., Yantosca, R. M., Savarino, J., Lee, C., and Thiemens, M.: Sulfate formation in sea - salt aerosols: Constraints from oxygen isotopes, *J. Geophys. Res.*, 110, D10307, 2005.
- Alexander, B., Park, R. J., Jacob, D. J., and Gong, S.: Transition metal - catalyzed oxidation of atmospheric sulfur: Global implications for the sulfur budget, *J. Geophys. Res.*, 114, D02309, 2009.
- Alexander, B., Allman, D., Amos, H., Fairlie, T., Dachs, J., Hegg, D. A., and Sletten, R. S.: Isotopic constraints on the formation pathways of sulfate aerosol in the marine boundary layer of the subtropical northeast Atlantic Ocean, *J. Geophys. Res.*, 117, D06304, 2012.
- Bao, H., Thiemens, M. H., Farquhar, J., Campbell, D. A., Lee, C. C.-W., Heine, K., and Loope, D. B.: Anomalous  $^{17}\text{O}$  compositions in massive sulphate deposits on the Earth, *Nature*, 406, 176-178, 2000.
- Bian, Y., Zhao, C., Ma, N., Chen, J., and Xu, W.: A study of aerosol liquid water content based on hygroscopicity measurements at high relative humidity in the North China Plain, *Atmos. Chem. Phys.*, 14, 6417-6426, 2014.
- Brook, R. D., Rajagopalan, S., Pope, C. A., Brook, J. R., Bhatnagar, A., Diez-Roux, A. V., Holguin, F., Hong, Y., Luepker, R. V., and Mittleman, M. A.: Particulate matter air pollution and cardiovascular disease an update to the scientific statement from the American Heart Association, *Circulation*, 121, 2331-2378, 2010.
- Calhoun, J. A., Bates, T. S., and Charlson, R. J.: Sulfur isotope measurements of submicrometer sulfate aerosol particles over the Pacific Ocean, *Geophys. Res. Lett.*, 18, 1877-1880, 1991.
- Chen, Q., Geng, L., Schmidt, J. A., Xie, Z., Kang, H., Dachs, J., Cole-Dai, J., Schauer, A. J., Camp, M. G., and Alexander, B.: Isotopic constraints on the role of hypohalous acids in sulfate aerosol formation in the remote marine boundary layer, *Atmos. Chem. Phys.*, 16, 11433-11450, 2016.
- Chen, Q., Schmidt, J. A., Shah, V., Jaeglé L., Sherwen, T., and Alexander, B.: Sulfate production by reactive bromine: Implications for the global sulfur and reactive bromine budgets, *Geophys. Res. Lett.*, 2017.
- Cheng, Y., Zheng, G., Wei, C., Mu, Q., Zheng, B., Wang, Z., Gao, M., Zhang, Q., He, K., and Carmichael, G.: Reactive nitrogen chemistry in aerosol water as a source of sulfate during haze events in China, *Sci. Adv.*, 2, e1601530, 2016.
- Cheng, Z., Jiang, J., Fajardo, O., Wang, S., and Hao, J.: Characteristics and health impacts of particulate matter pollution in China (2001–2011), *Atmos. Environ.*, 65, 186-194, 2013.
- Clifton, C. L., Altstein, N., and Huie, R. E.: Rate constant for the reaction of nitrogen dioxide with sulfur (IV) over the pH range 5.3-13, *Environ. Sci. Technol.*, 22, 586-589, 1988.



443 Dubey, M. K., Mohrschladt, R., Donahue, N. M., and Anderson, J. G.: Isotope specific kinetics of hydroxyl radical (OH)  
 444 with water (H<sub>2</sub>O): Testing models of reactivity and atmospheric fractionation, *J. Phys. Chem. A*, 101, 1494-1500, 1997.  
 445 Faloon, I.: Sulfur processing in the marine atmospheric boundary layer: A review and critical assessment of modeling  
 446 uncertainties, *Atmos. Environ.*, 43, 2841-2854, 2009.  
 447 Feingold, G., Frost, G. J., and Ravishankara, A.: Role of NO<sub>3</sub> in sulfate production in the wintertime northern latitudes, *J.*  
 448 *Geophys. Res.*, 107, 2002.  
 449 Fountoukis, C., and Nenes, A.: ISORROPIA II: a computationally efficient thermodynamic equilibrium model for K<sup>+</sup>-Ca<sup>2+</sup>-  
 450 Mg<sup>2+</sup>-NH<sub>4</sub><sup>+</sup>-Na<sup>+</sup>-SO<sub>4</sub><sup>2-</sup>-NO<sub>3</sub><sup>-</sup>-Cl<sup>-</sup>-H<sub>2</sub>O aerosols, *Atmos. Chem. Phys.*, 7, 4639-4659, 2007.  
 451 Fu, A.: Study on peroxides concentration and its influencing factors in the urban atmosphere, master of engineering, College  
 452 of Environmental and Resource Sciences, Zhejiang University, Hangzhou, China, 56 pp., 2014.(in Chinese)  
 453 Geng, L., Schauer, A. J., Kunasek, S. A., Sofen, E. D., Erbland, J., Savarino, J., Allman, D. J., Sletten, R. S., and Alexander,  
 454 B.: Analysis of oxygen - 17 excess of nitrate and sulfate at sub - micromole levels using the pyrolysis method, *Rapid*  
 455 *Commun. Mass Spectrom.*, 27, 2411-2419, 2013.  
 456 Guo, H., Weber, R. J., and Nenes, A.: High levels of ammonia do not raise fine particle pH sufficiently to yield nitrogen  
 457 oxide-dominated sulfate production, *Sci. Rep.*, 7, 12109, 2017.  
 458 Guo, J., Wang, Y., Shen, X., Wang, Z., Lee, T., Wang, X., Li, P., Sun, M., Collett, J. L., and Wang, W.: Characterization of  
 459 cloud water chemistry at Mount Tai, China: Seasonal variation, anthropogenic impact, and cloud processing, *Atmos.*  
 460 *Environ.*, 60, 467-476, 2012.  
 461 Guo, S., Hu, M., Zamora, M. L., Peng, J., Shang, D., Zheng, J., Du, Z., Wu, Z., Shao, M., and Zeng, L.: Elucidating severe  
 462 urban haze formation in China, *P. Natl. Acad. Sci. USA*, 111, 17373-17378, 2014.  
 463 Harris, E., Sinha, B., van Pinxteren, D., Tilgner, A., Fomba, K. W., Schneider, J., Roth, A., Gnauk, T., Fahlbusch, B., Mertes,  
 464 S., Lee, T., Collett, J., Foley, S., Borrmann, S., Hoppe, P., and Herrmann, H.: Enhanced Role of Transition Metal Ion  
 465 Catalysis During In-Cloud Oxidation of SO<sub>2</sub>, *Science*, 340, 727-730, 2013.  
 466 He, H., Wang, Y., Ma, Q., Ma, J., Chu, B., Ji, D., Tang, G., Liu, C., Zhang, H., and Hao, J.: Mineral dust and NO<sub>x</sub> promote  
 467 the conversion of SO<sub>2</sub> to sulfate in heavy pollution days, *Sci. Rep.*, 4, 4172, 2014.  
 468 Hennigan, C., Izumi, J., Sullivan, A., Weber, R., and Nenes, A.: A critical evaluation of proxy methods used to estimate the  
 469 acidity of atmospheric particles, *Atmos. Chem. Phys.*, 15, 2775-2790, 2015.  
 470 Hoffmann, M. R., and Calvert, J. G.: Chemical Transformation Modules for Eulerian Acid Deposition Models: Volume II,  
 471 the Aqueous-phase Chemistry, Atmospheric Sciences Research Laboratory, Office of Research and Development, US  
 472 Environmental Protection Agency, 1985.

473 Holt, B., Kumar, R., and Cunningham, P.: Oxygen-18 study of the aqueous-phase oxidation of sulfur dioxide, *Atmos.*  
474 *Environ.*, 15, 557-566, 1981.

475 Hung, H.-M., and Hoffmann, M. R.: Oxidation of gas-Phase SO<sub>2</sub> on the surfaces of acidic microdroplets: Implications for  
476 sulfate and sulfate radical anion formation in the atmospheric liquid phase, *Environ. Sci. Technol.*, 49, 13768-13776,  
477 2015.

478 Ibusuki, T., and Takeuchi, K.: Sulfur dioxide oxidation by oxygen catalyzed by mixtures of manganese (II) and iron (III) in  
479 aqueous solutions at environmental reaction conditions, *Atmos. Environ.*, 21, 1555-1560, 1987.

480 Ishino, S., Hattori, S., Savarino, J., Jourdain, B., Preunkert, S., Legrand, M., Caillon, N., Barbero, A., Kuribayashi, K., and  
481 Yoshida, N.: Seasonal variations of triple oxygen isotopic compositions of atmospheric sulfate, nitrate, and ozone at  
482 Dumont d'Urville, coastal Antarctica, *Atmos. Chem. Phys.*, 17, 3713-3727, 2017.

483 Jacob, D. J.: Heterogeneous chemistry and tropospheric ozone, *Atmos. Environ.*, 34, 2131-2159, 2000.

484 Jenkins, K. A., and Bao, H.: Multiple oxygen and sulfur isotope compositions of atmospheric sulfate in Baton Rouge, LA,  
485 USA, *Atmos. Environ.*, 40, 4528-4537, 2006.

486 Jiang, J., Zhou, W., Cheng, Z., Wang, S., He, K., and Hao, J.: Particulate matter distributions in China during a winter period  
487 with frequent pollution episodes (January 2013), *Aerosol Air Qual. Res.*, 15, 494-503, 2015.

488 Lee, C. W., Savarino, J., Cachier, H., and Thiemens, M.: Sulfur (<sup>32</sup>S, <sup>33</sup>S, <sup>34</sup>S, <sup>36</sup>S) and oxygen (<sup>16</sup>O, <sup>17</sup>O, <sup>18</sup>O) isotopic ratios  
489 of primary sulfate produced from combustion processes, *Tellus B*, 54, 193-200, 2002.

490 Lee, Y. N., and Schwartz, S. E.: Kinetics of oxidation of aqueous sulfur (IV) by nitrogen dioxide, in: *Kinetics of oxidation of*  
491 *aqueous sulfur (IV) by nitrogen dioxide, Precipitation scavenging, dry Deposition and resuspension*, California, 1982,  
492 453-470, 1983.

493 Legrand, M., Hammer, C., De Angelis, M., Savarino, J., Delmas, R., Clausen, H., and Johnsen, S. J.: Sulfur - containing  
494 species (methanesulfonate and SO<sub>4</sub>) over the last climatic cycle in the Greenland Ice Core Project (central Greenland)  
495 ice core, *J. Geophys. Res.*, 102, 26663-26679, 1997.

496 Legrand, M., and Mayewski, P.: Glaciochemistry of polar ice cores: A review, *Rev. Geophys.*, 35, 219-243, 1997.

497 Li, L., Chen, Z., Zhang, Y., Zhu, T., Li, J., and Ding, J.: Kinetics and mechanism of heterogeneous oxidation of sulfur  
498 dioxide by ozone on surface of calcium carbonate, *Atmos. Chem. Phys.*, 6, 2453-2464, 2006.

499 Li, X., Bao, H., Gan, Y., Zhou, A., and Liu, Y.: Multiple oxygen and sulfur isotope compositions of secondary atmospheric  
500 sulfate in a mega-city in central China, *Atmos. Environ.*, 81, 591-599, 2013.

501 Lin, M., Biglari, S., Zhang, Z., Crocker, D., Tao, J., Su, B., Liu, L., and Thiemens, M. H.: Vertically uniform formation  
502 pathways of tropospheric sulfate aerosols in East China detected from triple stable oxygen and radiogenic sulfur  
503 isotopes, *Geophys. Res. Lett.*, 2017.

504 Liu, M., Song, Y., Zhou, T., Xu, Z., Yan, C., Zheng, M., Wu, Z., Hu, M., Wu, Y., and Zhu, T.: Fine Particle pH during  
 505 Severe Haze Episodes in Northern China, *Geophys. Res. Lett.*, 2017.

506 Liu, X., and Millero, F. J.: The solubility of iron hydroxide in sodium chloride solutions, *Geochim. Cosmochim. Acta*, 63,  
 507 3487-3497, 1999.

508 Luz, B., and Barkan, E.: The isotopic ratios  $^{17}\text{O}/^{16}\text{O}$  and  $^{18}\text{O}/^{16}\text{O}$  in molecular oxygen and their significance in  
 509 biogeochemistry, *Geochim. Cosmochim. Acta*, 69, 1099-1110, 2005.

510 Martin, L. R., and Hill, M. W.: The iron catalyzed oxidation of sulfur: Reconciliation of the literature rates, *Atmos. Environ.*,  
 511 21, 1487-1490, 1967.

512 Matsuhisa, Y., Goldsmith, J. R., and Clayton, R. N.: Mechanisms of hydrothermal crystallization of quartz at 250 °C and 15  
 513 kbar, *Geochim. Cosmochim. Acta*, 42, 173-182, 1978.

514 McArdle, J. V., and Hoffmann, M. R.: Kinetics and mechanism of the oxidation of aquated sulfur dioxide by hydrogen  
 515 peroxide at low pH, *J. Phys. Chem.*, 87, 5425-5429, 1983.

516 Meng, Z., Lin, W., Jiang, X., Yan, P., Wang, Y., Zhang, Y., Jia, X., and Yu, X.: Characteristics of atmospheric ammonia  
 517 over Beijing, China, *Atmos. Chem. Phys.*, 11, 6139-6151, 2011.

518 Rood, M., Shaw, M., Larson, T., and Covert, D.: Ubiquitous nature of ambient metastable aerosol, *Nature*, 337, 537-539,  
 519 1989.

520 Savarino, J., and Thiemens, M. H.: Analytical procedure to determine both  $\delta^{18}\text{O}$  and  $\delta^{17}\text{O}$  of  $\text{H}_2\text{O}_2$  in natural water and first  
 521 measurements, *Atmos. Environ.*, 33, 3683-3690, 1999.

522 Savarino, J., Lee, C. C., and Thiemens, M. H.: Laboratory oxygen isotopic study of sulfur (IV) oxidation: Origin of the  
 523 mass - independent oxygen isotopic anomaly in atmospheric sulfates and sulfate mineral deposits on Earth, *J. Geophys.*  
 524 *Res.*, 105, 29079-29088, 2000.

525 Savarino, J., Alexander, B., Darmohusodo, V., and Thiemens, M. H.: Sulfur and oxygen isotope analysis of sulfate at  
 526 micromole levels using a pyrolysis technique in a continuous flow system, *Anal. Chem.*, 73, 4457-4462, 2001.

527 Seinfeld, J. H., and Pandis, S. N.: *Atmospheric chemistry and physics: From air pollution to climate change*, John Wiley &  
 528 Sons, New Jersey, 2012.

529 Shen, C. H., and Rochelle, G. T.: Nitrogen dioxide absorption and sulfite oxidation in aqueous sulfite, *Environ. Sci. Technol.*,  
 530 32, 1994-2003, 1998.

531 Shen, X., Lee, T., Guo, J., Wang, X., Li, P., Xu, P., Wang, Y., Ren, Y., Wang, W., and Wang, T.: Aqueous phase sulfate  
 532 production in clouds in eastern China, *Atmos. Environ.*, 62, 502-511, 2012.

533 Sofen, E., Alexander, B., Steig, E., Thiemens, M., Kunasek, S., Amos, H., Schauer, A., Hastings, M., Bautista, J., and  
534 Jackson, T.: WAIS Divide ice core suggests sustained changes in the atmospheric formation pathways of sulfate and  
535 nitrate since the 19th century in the extratropical Southern Hemisphere, *Atmos. Chem. Phys.*, 14, 5749-5769, 2014.

536 Sun, Y., Zhuang, G., Tang, A., Wang, Y., and An, Z.: Chemical characteristics of PM<sub>2.5</sub> and PM<sub>10</sub> in haze-fog episodes in  
537 Beijing, *Environ. Sci. Technol.*, 40, 3148-3155, 2006.

538 Vicars, W. C., and Savarino, J.: Quantitative constraints on the 17O-excess ( $\Delta^{17}\text{O}$ ) signature of surface ozone: Ambient  
539 measurements from 50 °N to 50 °S using the nitrite-coated filter technique, *Geochim. Cosmochim. Acta*, 135, 270-287,  
540 2014.

541 Walcek, C. J., and Taylor, G. R.: A theoretical method for computing vertical distributions of acidity and sulfate production  
542 within cumulus clouds, *J. Atmos. Sci.*, 43, 339-355, 1986.

543 Wang, G., Zhang, R., Gomez, M. E., Yang, L., Zamora, M. L., Hu, M., Lin, Y., Peng, J., Guo, S., and Meng, J.: Persistent  
544 sulfate formation from London Fog to Chinese haze, *P. Natl. Acad. Sci. USA*, 113, 13630-13635, 2016.

545 Wang, Y., Zhuang, G., Tang, A., Yuan, H., Sun, Y., Chen, S., and Zheng, A.: The ion chemistry and the source of PM<sub>2.5</sub>  
546 aerosol in Beijing, *Atmos. Environ.*, 39, 3771-3784, 2005.

547 Wang, Y., Zhang, Q., Jiang, J., Zhou, W., Wang, B., He, K., Duan, F., Zhang, Q., Philip, S., and Xie, Y.: Enhanced sulfate  
548 formation during China's severe winter haze episode in January 2013 missing from current models, *J. Geophys. Res.*,  
549 119, 10425-10440, 2014.

550 Ye, P., Xie, Z., Yu, J., and Kang, H.: Spatial distribution of methanesulphonic acid in the Arctic aerosol collected during the  
551 Chinese Arctic Research Expedition, *Atmosphere*, 6, 699-712, 2015.

552 Zheng, B., Zhang, Q., Zhang, Y., He, K., Wang, K., Zheng, G., Duan, F., Ma, Y., and Kimoto, T.: Heterogeneous chemistry:  
553 a mechanism missing in current models to explain secondary inorganic aerosol formation during the January 2013 haze  
554 episode in North China, *Atmos. Chem. Phys.*, 15, 2031-2049, 2015a.

555 Zheng, G., Duan, F., Su, H., Ma, Y., Cheng, Y., Zheng, B., Zhang, Q., Huang, T., Kimoto, T., and Chang, D.: Exploring the  
556 severe winter haze in Beijing: the impact of synoptic weather, regional transport and heterogeneous reactions, *Atmos.*  
557 *Chem. Phys.*, 15, 2969-2983, 2015b.

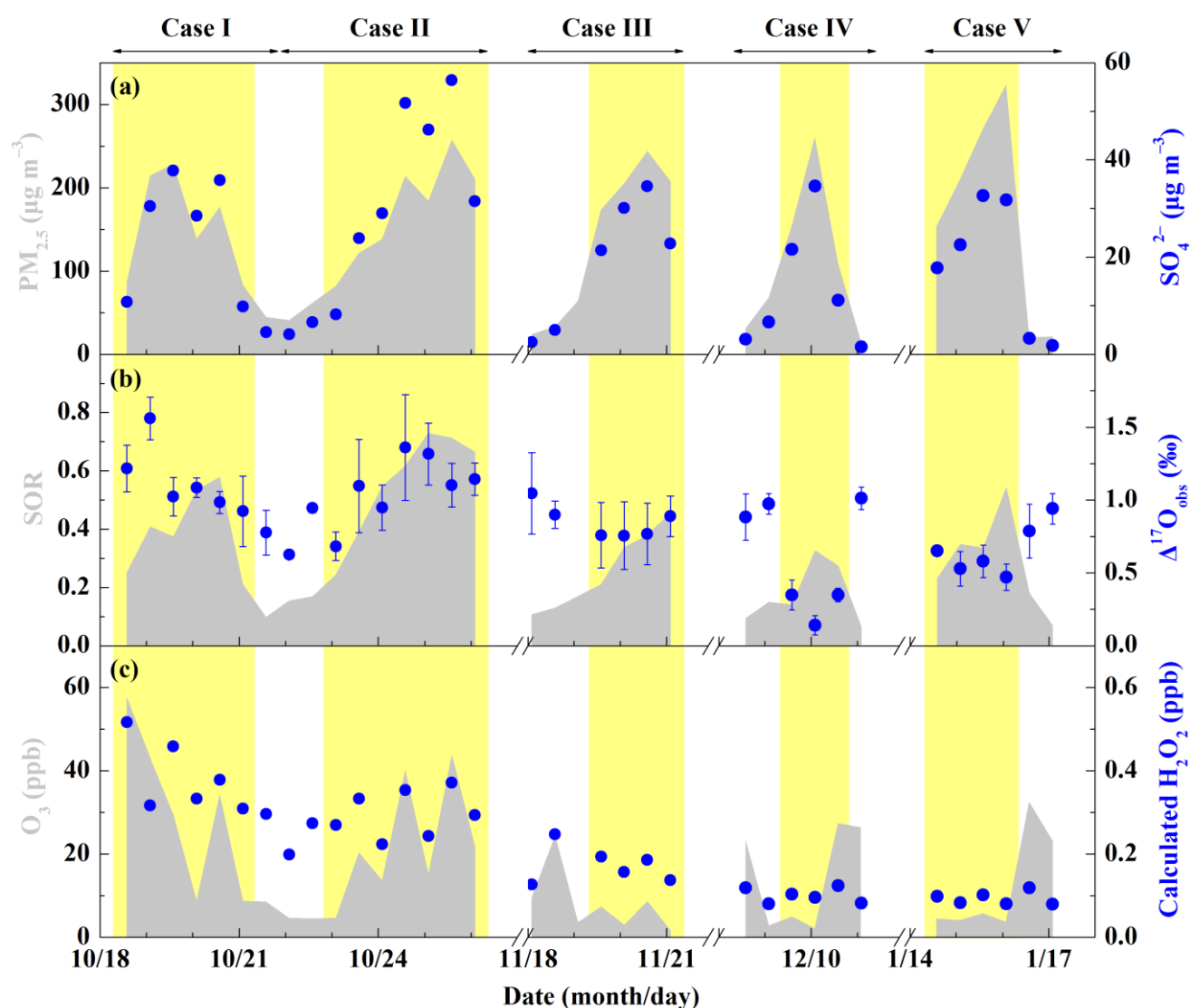
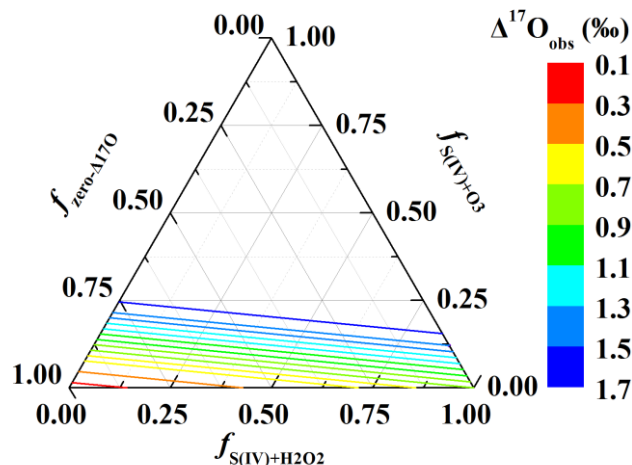


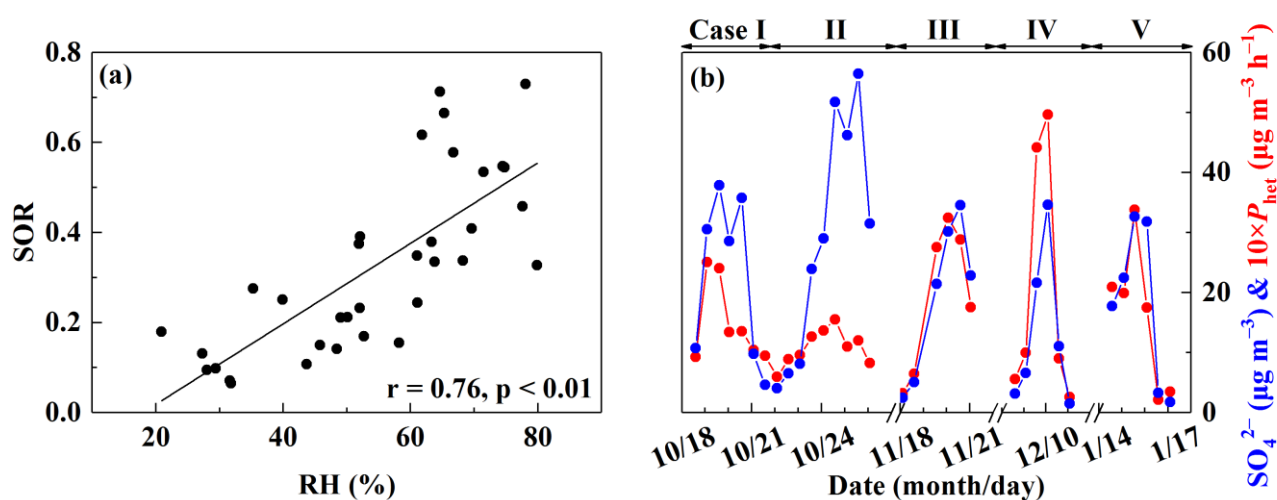
**Figure 1.** Characteristics of haze events in Beijing (October 2014–January 2015). (a) Temporal evolution of  $\text{PM}_{2.5}$  and  $\text{SO}_4^{2-}$  concentrations. (b) Temporal evolution of sulfur oxidation ratio ( $\text{SOR} = n\text{SO}_4^{2-}/(n\text{SO}_4^{2-} + n\text{SO}_2)$ ,  $n$  represents the molar concentration) and observed  $\Delta^{17}\text{O}(\text{SO}_4^{2-})$  ( $\Delta^{17}\text{O}_{\text{obs}}$ ). (c) Temporal evolution of observed  $\text{O}_3$  and calculated  $\text{H}_2\text{O}_2$ . The error bar of  $\Delta^{17}\text{O}_{\text{obs}}$  in (b) is  $\pm 1\sigma$  of replicate measurements ( $n = 2\text{--}4$ ) of each sample. The light yellow shaded area indicates polluted days (PD,  $\text{PM}_{2.5} \geq 75 \mu\text{g m}^{-3}$ ). Data used here are 12h-averaged values, corresponding with filter samples.



566

567 **Figure 2.** Ternary diagram of possible fractional contribution of different pathways to total sulfate production directly  
 568 estimated from  $\Delta^{17}\text{O}_{\text{obs}}$ . The colored lines are contour lines of  $\Delta^{17}\text{O}_{\text{obs}}$ , representing possible fractional contribution of sulfate  
 569 formation via  $\text{O}_3$  ( $f_{\text{S(IV)}+\text{O}_3}$ ) and  $\text{H}_2\text{O}_2$  ( $f_{\text{S(IV)}+\text{H}_2\text{O}_2}$ ) oxidation or zero- $\Delta^{17}\text{O}$  processes ( $f_{\text{zero}-\Delta^{17}\text{O}}$ ) such as primary sulfate, secondary  
 570 sulfate formed via OH oxidation,  $\text{NO}_2$  oxidation and  $\text{O}_2$  oxidation.

571



572

573 **Figure 3.** The relationship between RH and SOR (a) and time series of overall heterogeneous sulfate production ( $P_{\text{het}}$ ) along  
 574 with  $\text{SO}_4^{2-}$  concentrations (b). The black line in (a) is linear least-squares fitting line.

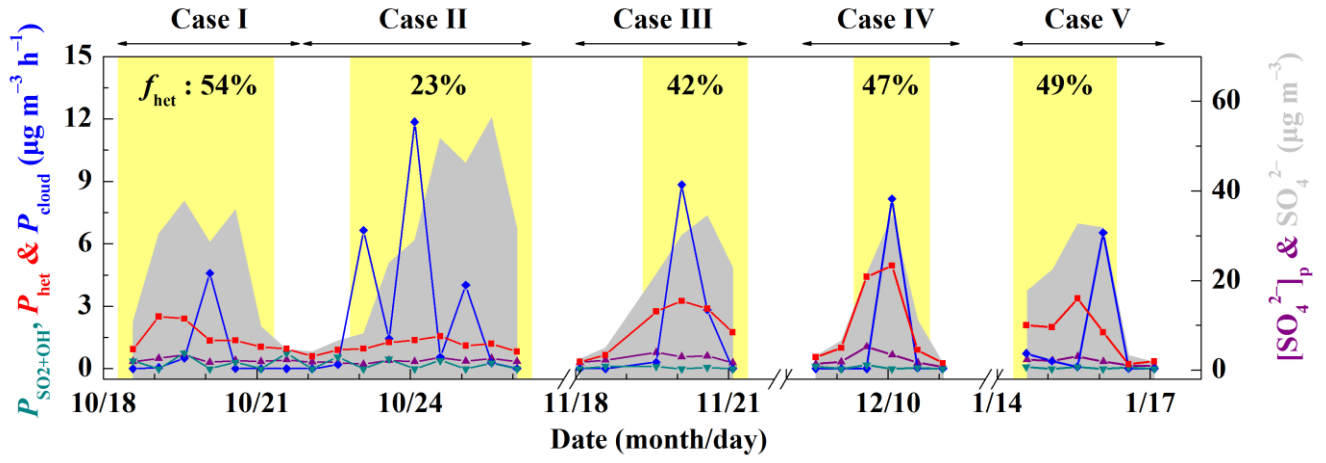


**Figure 4.** Estimate of different sulfate production pathways. Time series of estimated sulfate production rate via OH oxidation in the gas-phase ( $P_{\text{SO}_2+\text{OH}}$ ), overall heterogeneous reactions on aerosols ( $P_{\text{het}}$ ) and in-cloud reactions ( $P_{\text{cloud}}$ ) and concentrations of primary sulfate ( $[\text{SO}_4^{2-}]_p$ ) and observed sulfate.  $f_{\text{het}}$  represents the fraction of overall heterogeneous sulfate production to total sulfate production during PD of each Case. The light yellow shaded area indicates polluted days (PD,  $\text{PM}_{2.5} \geq 75 \mu\text{g m}^{-3}$ ). Data used here are 12h-averaged values, corresponding with filter samples.

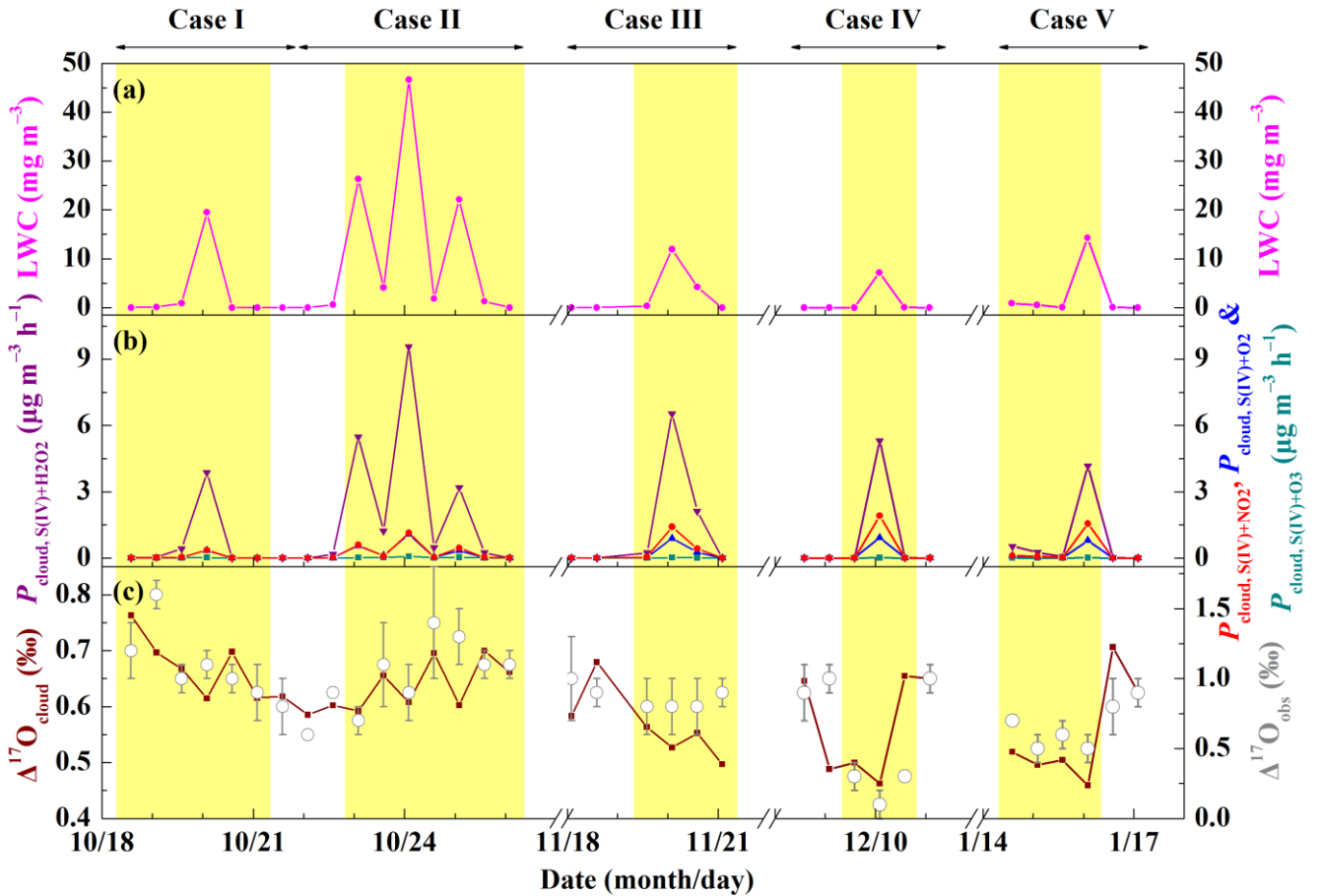
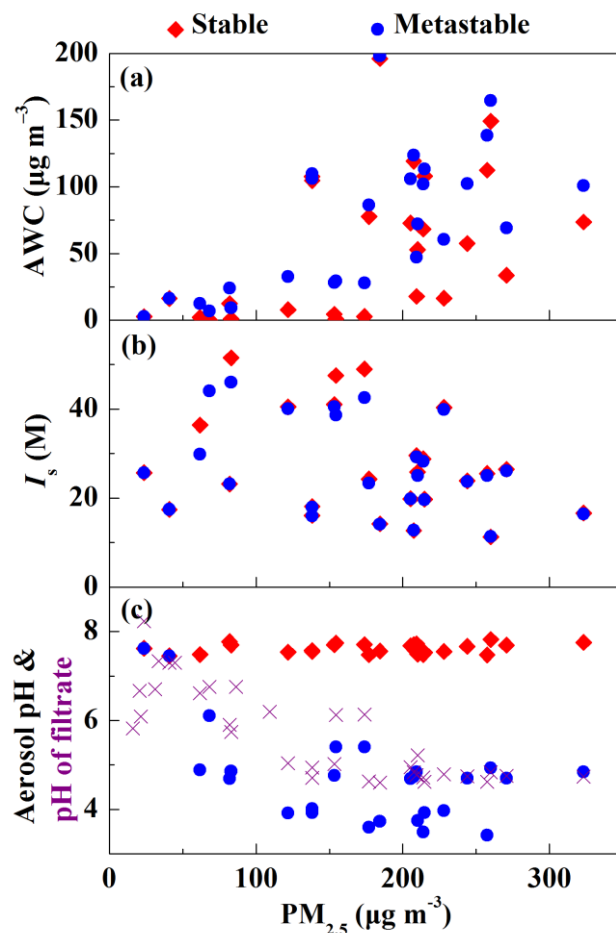


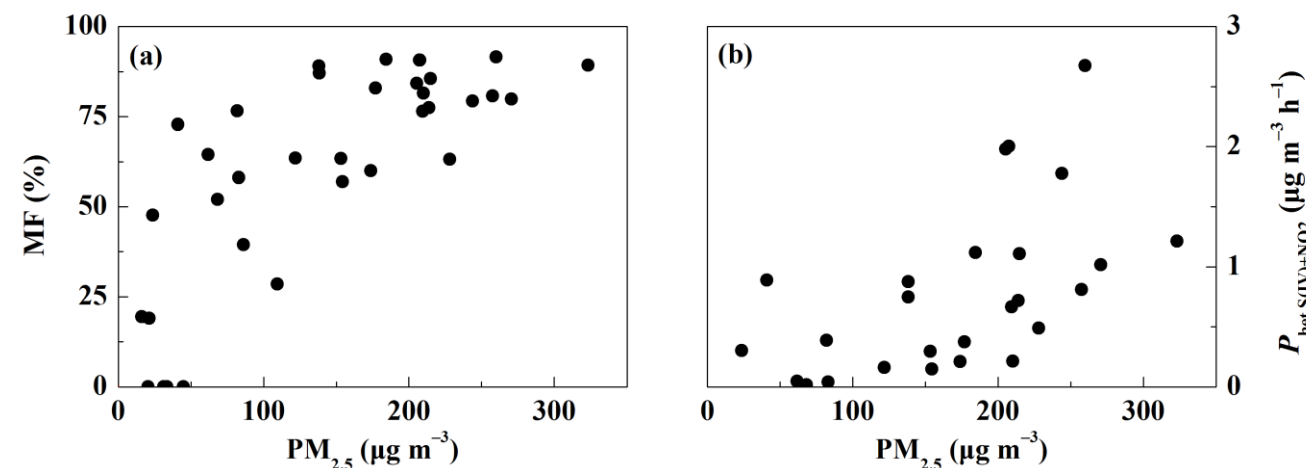
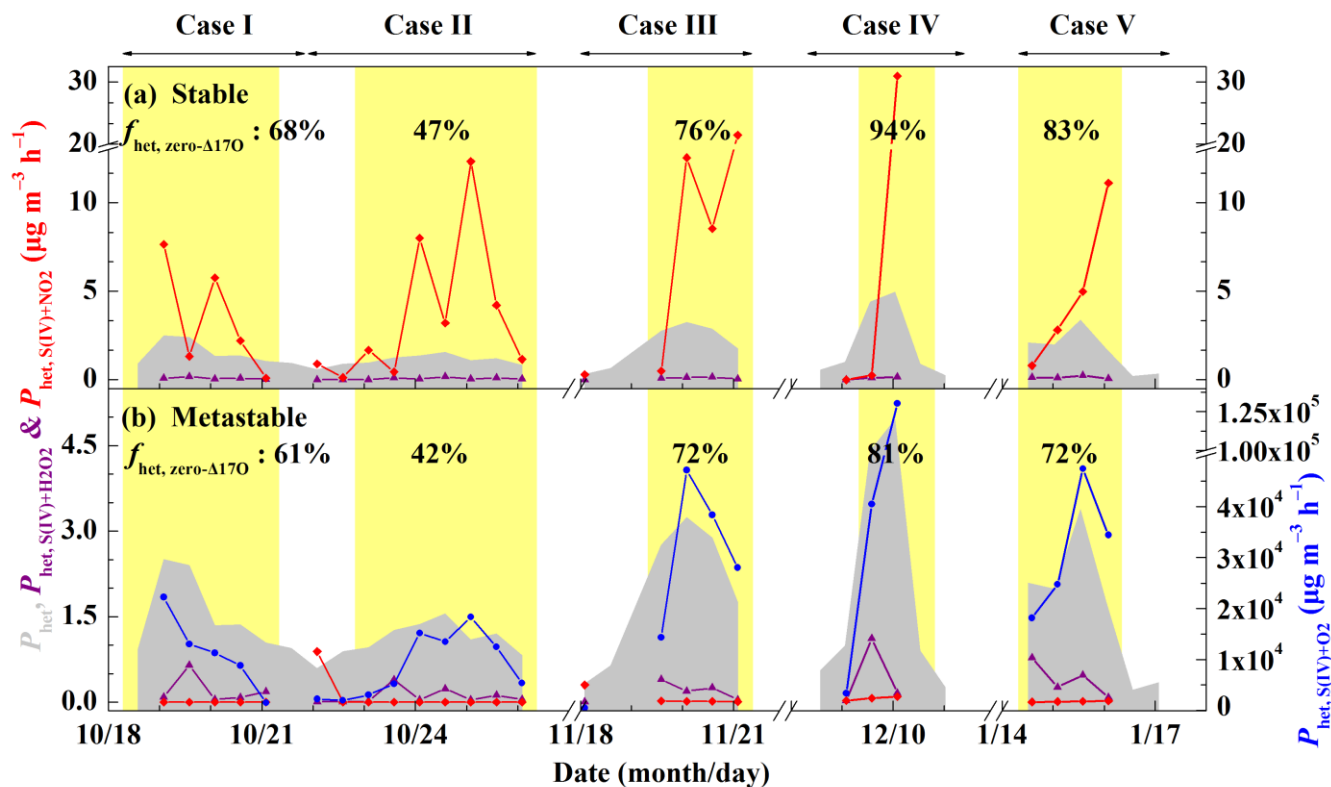
**Figure 5.** Temporal evolution of cloud liquid water content (LWC, a), in-cloud sulfate production rate via S(IV) oxidation by  $\text{H}_2\text{O}_2$ ,  $\text{O}_3$ ,  $\text{NO}_2$  and  $\text{O}_2$  initiated by TMIs (denoted as  $P_{\text{cloud, S(IV)+H}_2\text{O}_2}$ ,  $P_{\text{cloud, S(IV)+O}_3}$ ,  $P_{\text{cloud, S(IV)+NO}_2}$  and  $P_{\text{cloud, S(IV)+O}_2}$ , respectively,



584 **b)** and estimated  $\Delta^{17}\text{O}$  of sulfate produced in clouds ( $\Delta^{17}\text{O}_{\text{cloud}}$ , **c**). The light yellow shaded area indicates polluted days (PD,  
 585  $\text{PM}_{2.5} \geq 75 \mu\text{g m}^{-3}$ ). Data used here are 12h-averaged values, corresponding with filter samples.



586  
 587 **Figure 6.** Aerosol parameters during Beijing haze. The aerosol water content (AWC, **a**), ionic strength ( $I_s$ , **b**) and aerosol pH  
 588 (**c**) was predicted by ISORROPIA II assuming stable aerosol state and metastable aerosol state. The pH of filtrate was  
 589 measured by an ion activity meter.



602 **Figure 8.** The estimated fraction of metastable aerosol to total aerosol (MF, **a**) using Eq. (9) and heterogeneous sulfate  
 603 production rate from S(IV) oxidation by NO<sub>2</sub> assuming a combination of metastable and stable state ( $P_{\text{het, S(IV)+NO}_2}$ , **b**) as  $P_{\text{het, S(IV)+NO}_2}$   
 604  $P_{\text{het, S(IV)+NO}_2} = \text{MF} \times P_{\text{het, S(IV)+NO}_2, \text{metastable}} + (100 \% - \text{MF}) \times P_{\text{het, S(IV)+NO}_2, \text{stable}}$ .

605 **Table 1.** Sulfate isotope assumptions.

Sulfate formation pathways	$\Delta^{17}\text{O}(\text{SO}_4^{2-})$ (‰)
SO <sub>2</sub> + OH	0
S(IV) + H <sub>2</sub> O <sub>2</sub>	0.7
S(IV) + O <sub>3</sub>	6.5
S(IV) + NO <sub>2</sub>	0
S(IV) + O <sub>2</sub>	0
Primary sulfate	0

606